



Subsurface geological and geophysical data from the Po Plain and the northern Adriatic Sea (north Italy)

Michele Livani¹, Lorenzo Petracchini¹, Christoforos Benetatos², Francesco Marzano², Andrea Billi¹,
Eugenio Carminati³, Carlo Doglioni^{3,4}, Patrizio Petricca⁵, Roberta Maffucci^{3,4}, Giulia Codegone²,
Vera Rocca², Francesca Verga², and Ilaria Antoncetti⁶

¹Consiglio Nazionale delle Ricerche, IGAG, Rome, Italy

²Dipartimento di Ingegneria dell'Ambiente, del Territorio e delle Infrastrutture,
Politecnico di Torino, Torino, Italy

³Dipartimento di Scienze della Terra, Sapienza Università di Roma, Rome, Italy

⁴Istituto Nazionale di Geofisica e Vulcanologia, Rome, Italy

⁵ISPRA Servizio Geologico d'Italia, Via Vitaliano Brancati, 48, 00144 Rome, Italy

⁶Direzione Generale per le Infrastrutture e la Sicurezza, Ministero della Transizione Ecologica, Rome, Italy

Correspondence: Lorenzo Petracchini (lorenzo.petracchini@cnr.it)

Received: 19 February 2023 – Discussion started: 6 March 2023

Revised: 8 July 2023 – Accepted: 29 July 2023 – Published: 28 September 2023

Abstract. The Po Plain (Italy) is one of the most densely populated and productive regions of Europe, characterized by a flourishing economy (also linked to strategic subsurface resources) and several world cultural and natural heritage sites. The coupling of socio-economic interests with geological hazards (i.e. seismic, subsidence, and flooding hazards) in this area requires accurate knowledge of the subsurface geology, the active geological processes, and the impact of human activities on natural environments to mitigate the potential natural and anthropic risks.

Most data unveiling the subsurface geology of this region were produced by the hydrocarbon exploration industry. Indeed, the Po Plain hosts many hydrocarbon fields that have been discovered since the early 1950s, giving rise to the subsurface exploration through extensive seismic reflection surveys and drilling of numerous deep wells. In this work, geological and geophysical data from 160 deep wells drilled for hydrocarbon exploration and/or exploitation purposes in the Po Plain and in the facing northern Adriatic Sea have been collected and digitized along with several published geological cross-sections and maps. These data have been used to reconstruct the overall subsurface 3D architecture and to extract the physical properties of the subsurface geological units.

The digitized data are suitable to be imported into geo-software environments so as to derive the geophysical and mechanical properties of the geological units for a wealth of applied and scientific studies such as geomechanical, geophysical, and seismological studies.

The integrated dataset may represent a useful tool in defining regional first-order strategies to ensure the safety of the urbanized areas and human activities and to reduce natural and anthropic risks that may affect this crucial region of Europe. In particular, the data collected would be useful to highlight sensible areas where data collection and more detailed studies are needed. Nowadays, such issues are particularly relevant for the underground industry development related to the increasing interest in possible CO₂ and hydrogen underground storage, which can play a fundamental role in the energy transition process towards decarbonization goals. The full dataset is available at the following link: <https://doi.org/10.5281/zenodo.8126519> (Livani et al., 2023).

1 Introduction

The Po Plain in the north of Italy is the most productive and prosperous region of Italy (Fig. 1a), with a per-capita income similar to that of central and northern European countries (<https://ec.europa.eu/eurostat>, last access: 8 July 2022; Helliwell and Putnam, 1995; Tabellini, 2010; European Commission, 2016). The area is densely populated (<https://ec.europa.eu/eurostat>, last access: 8 July 2022; Fig. 1a) and hosts numerous UNESCO world heritage sites such as the cities of Venice, Verona, Bergamo, and Ravenna (<https://whc.unesco.org/>, last access: 13 December 2022; Fig. 1b).

Since the second half of the 20th century, the discovery and exploitation of numerous hydrocarbon (mostly gas) resources contributed to the economic development of Italy. Indeed, the Po Plain and the facing northern Adriatic Sea host the majority of hydrocarbon fields in the country (extracting almost 33 % of the total national gas production) and most of the Italian underground gas storage sites, which have been operative since the 1960s (<https://unmig.mise.gov.it/>, last access: 9 January 2023; Fig. 1b).

The Eni-AGIP Company hydrocarbon exploration and exploitation activities in the Po Plain and northern Adriatic Sea led to the production of a large amount of subsurface data, which include: (i) seismic data acquired through extensive regional 2D and 3D seismic surveys for the development of onshore and offshore hydrocarbon fields and (ii) well data acquired during the drilling of explorative and developmental wells. The subsurface dataset provided structural, stratigraphic, and sedimentological information, which allowed the obtainment of accurate knowledge of the regional subsurface architecture and geological evolution (e.g. Pieri and Groppi, 1981; Cassano et al., 1986; Casero, 2004; Ghielmi et al., 2010, 2013; Fantoni and Franciosi, 2009, 2010).

The geological evolution of the Po Plain is accompanied by seismic, subsidence, and flooding events that are the main phenomena to consider in natural-hazard assessments. The cultural, social, and economic relevance of this region demands a careful evaluation of both natural hazards and human activities to mitigate the potential correlated risks and to guarantee the safety of the urbanized areas and human activities themselves.

The Po Plain is characterized by moderate seismicity (International Commission on Hydrocarbon Exploration and Seismicity in the Emilia region, 2014). Nonetheless, instrumental and historical intermediate–strong ($M_w \geq 5.0$) earthquakes hit the area (Rovida et al., 2022), such as the events that occurred in 1117 (M_w 6.5; Verona area); in 1570 (M_w 5.6; Ferrara area); and 2012, when a seismic sequence in the Modena and Ferrara provinces occurred (main shock M_w 6.09). The latter event promoted the implementation of the seismic monitoring network as an essential instrument for the safe management of industrial activities. Notice that no case of anthropogenically induced seismicity has been documented so far in the study area (Braun et al., 2020).

The Po Plain is also characterized by significant subsidence of both natural and anthropic origin; this became particularly intense after the economic growth following World War II. The natural component is the result of several geological processes, such as sediment load and compaction, vertical tectonic movements, and rebound effects after the last deglaciation (Carminati and Di Donato, 1999). Anthropogenic subsidence is primarily influenced by groundwater withdrawal for industrial, agricultural, and civil uses (e.g. Herrera-Garcia et al., 2021). Subordinately, it is linked to hydrocarbon (mainly gas) exploitation from onshore and offshore reservoirs (Carminati and Martinelli, 2002; Bitelli et al., 2020).

Subsidence mainly affects the central and eastern sectors of the Po Plain: the highest total subsidence rates, greater than -60 mm yr^{-1} , were evaluated for the Bologna city area (Carminati and Martinelli, 2002; Zerbini et al., 2007; Baldi et al., 2009), whereas the highest natural component reaches -2.0 mm yr^{-1} at the Pede–Apennine zone, near the city of Bologna. The difference between the total (natural plus anthropogenic) vs. natural components of the present-day subsidence shows that the main factor controlling modern subsidence in this region is anthropogenic (Carminati and Martinelli, 2002).

Subsidence is monitored through the implementation of different technologies (GPS, InSAR (interferometric synthetic aperture radar), levelling surveys) that are useful for the prevention, mitigation, and control of the natural processes, as well as of the human ones (e.g. Dacome et al., 2015; Benetatos et al., 2020).

Flood events related to the Po River (which crosses the whole Po Plain) and its tributaries represent an additional natural risk (Domeneghetti et al., 2015, and references therein). In the past century, the worldwide increase of flood susceptibility and risk increased together with the rise of subsidence due to groundwater depletion (e.g. Herrera-Garcia et al., 2021). In the Po Plain, subsidence and flood hazards are presumably linked since there is a clear-cut correlation between high flood frequency and rapid subsidence, whereas only a few floods occurred in low-subsidence areas (Carminati and Martinelli, 2002). Nevertheless, in the first half of 2022, the most significant drought of at least 70 years was observed for the area, causing extensive damage to agriculture and encouraging the entry of the saline wedge at the mouth of the Po River along the Adriatic coast.

The protection of the cultural, social, and economic heritage of the Po Plain makes the adoption of all available measures necessary to reduce the impact of natural and anthropic-derived hazards in the study area.

To this end, the definition of the physical and geometrical attributes of the outcropping and subsurface geological units provides fundamental knowledge for several scientific issues and could be used in a preliminary definition of engineering operations. As an example, the integration of physical parameters of subsurface geological units into a well-defined 3D

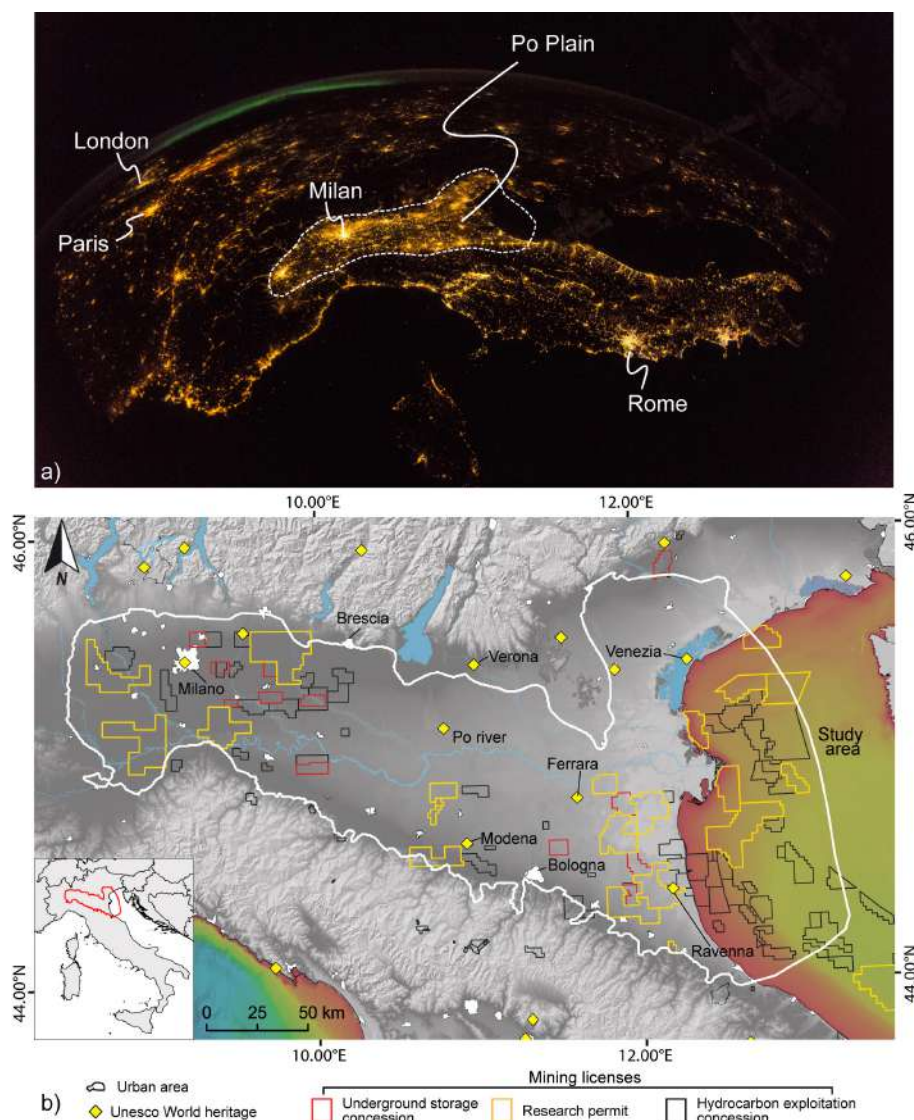


Figure 1. (a) Modified photo taken by the ESA astronaut Alexander Gerst, snapped from the International Space Station, that clearly reveals the high-density population in the Po Plain area highlighted by the strong night-light intensity (credit: ESA/NASA – CC BY-SA IGO 3.0; the original photo has been modified). (b) The figure shows the main cities in the Po Plain, the UNESCO world heritages (data from <https://whc.unesco.org/>, last access: 13 December 2022), and the current mining licenses (data from <https://unmig.mise.gov.it/>, last access: 9 January 2023).

model can be applied to (i) reduce the uncertainties for earthquake location, contributing to the calculation of more accurate focal mechanisms and performing wave propagation and ground motion simulations (e.g. Magistrale et al., 1996; Süß et al., 2001; Molinari et al., 2015; Livani et al., 2022); and (ii) understand, simulate, and predict the response of the geological body to subsurface natural and anthropic processes. The latter is the case for 3D geomechanical numerical models, which represent effective tools for the evaluation and prediction of the possible effects – both at the surface and in the subsurface – of geofluid extraction and storage to guarantee the safe management of such activities, as well as to quan-

tify and better understand the ongoing geological processes (e.g. tectonic deformation and natural subsidence; Teatini et al., 2006; Codegone et al., 2016; Benetatos et al., 2020). As an example, numerical models can play a fundamental role during the geological sequestration of CO₂ and gas storage (e.g. hydrogen as an energy carrier) in natural underground formations since they are mandatory for the optimization of the development strategies, the maximization of storage efficiency, and monitoring activities.

In this paper, we present an integrated database of geological and geophysical data regarding the subsurface of the Po Plain and the facing Adriatic Sea. The database provides

a collection of data distinguished as primitive and derived. The primitive data consist of a detailed and accurate collection and digitization of subsurface information extracted from wells, geological cross-sections, and geological maps. The derived data are obtained from the revision and processing of the primitive data and by gridded surfaces representing the main geological units of the Po Plain subsurface.

It is worth mentioning that, in the study area, the geological literature offering interpretations of the subsoil is abundant in terms of geological reconstructions. Our database represents a collection of the main published works regarding the Po Plain. Detailed studies related to specific sectors of the Po Plain might not be present in our database. Recently, other subsurface geological models have been elaborated upon, providing several isobath maps of the Po Plain (e.g. Turrini et al., 2014; ISPRA, 2015; Molinari et al., 2015; Amadori et al., 2019; D'Ambrogi et al., 2023). It is worth mentioning two projects: the recent GO-PEG project (D'Ambrogi et al., 2023), which provides the geometry of four stratigraphic horizons in the Po Plain area deriving from the GeoMol project (<http://www.geomol.eu>, last access: 30 June 2023; ISPRA, 2015; Maesano and D'Ambrogi, 2016) and the GeoERA-HotLime project (<https://geoera.eu/projects/hotlime6/>, last access: 30 June 2023), and the Mambo project (Molinari et al., 2015), which covers almost the entire Po Plain. In our work, due to technical difficulties (e.g. the impossibility of precisely defining the depth reported in the maps), we were not able to integrate all the previous datasets. Anyhow, where possible, we integrated the available regional geological models with other primitive public data to coherently define the geometry of five surfaces of the Po Plain subsurface, which are, from the oldest to the youngest, as follows: the magnetic basement top, the top of the carbonate succession, the Pliocene base, the Calabrian base, and the base of recent continental deposits. The above-mentioned surfaces represent lithological boundaries rather than chronostratigraphic or formational limits, defining units that are expected to show different mechanical behaviour. Most importantly, the gridded surfaces of our dataset come with a series of detailed geophysical and geological parameters extracted from the composite logs of deep wells (i.e. the primitive data). In addition to the geophysical and geological data, a statistical analysis is reported and discussed as a preliminary elaboration of the collected data.

We believe that our dataset provides an important contribution to a broad audience of policymakers and scientists for understanding and evaluating geological and anthropic processes in the area, for setting secure development strategies for correct territory management, and for the reduction of social and economic risks in a strategic area for Italy and Europe.

2 Geological setting

The Po Plain and the facing Adriatic Sea lie on the buried sector of the Adria microplate, a promontory of the Africa plate or an independent microplate, interposed between the NE-verging northern Apennines and the S-verging southern Alps (Fig. 2; Dercourt et al., 1986; Pieri and Groppi, 1981; Castellarin et al., 1985; Castellarin and Vai, 1986; Doglioni, 1993; Carminati et al., 2003; Carminati and Doglioni, 2012; Fantoni and Franciosi, 2009, 2010; Turrini et al., 2016; Pezzo et al., 2020). The development of these two facing fold-and-thrust belts, connected with the broad collision of the Eurasian and African plates, led to the formation of the Po Plain basin representing the foreland basin of both orogens. Compressional tectonics have affected the area since the middle Eocene time, with the development of WNW–ESE-oriented thrusts in the southern Alps followed, from the Oligocene–lower Miocene onward, by the NW–SE-oriented thrust system of the northern Apennines (Coward and Dietrich, 1989; Carminati and Doglioni, 2012; Carminati et al., 2012; Maesano and D'Ambrogi, 2016).

The structural and sedimentary framework of the area has been constrained using numerous seismic reflection profiles and deep-well logs (e.g. Pieri, 1983; Cassano et al., 1986; Fantoni and Franciosi, 2010; Turrini et al., 2014; ISPRA, 2015; Livani et al., 2018; Amadori et al., 2019; D'Ambrogi et al., 2023, and references therein).

The Apennines front is characterized by three main orogenic arcs from west to east: Monferrato, Emilia, and Ferrara arcs (Fig. 2a). The southern Alps represent the non-metamorphic retrobelt of the double-verging Alpine chain, and, on the western side of the study area, it reaches the southernmost extent with its edge very close to the northern Apennines front (Ravaglia et al., 2006; Fantoni and Franciosi, 2010; Toscani et al., 2014; Fig. 2b). The external fronts of the two facing chains are mostly buried under a siliciclastic sequence (late Eocene–actual) consisting of syn-tectonic sediments and recent alluvial sediments of the Po River (Pieri and Groppi, 1981; Boccaletti et al., 1985; Bigi et al., 1990a, b; Fantoni and Franciosi, 2010; Ghielmi et al., 2010, 2013; Carminati and Doglioni, 2012; Amadori et al., 2019, and references therein). In detail, the siliciclastic sequence (Fig. 3) can be subdivided into a lower (late Eocene–early Messinian) and an upper (late Messinian–present) cycle (Ricci Lucchi, 1986). The lower cycle, primarily fed by the Alpine chain, consists of silty and shaly deposits (i.e. Gallare Marls; late Eocene to Miocene time) in places intercalated by or interdigitated with sandy and conglomeratic deposits (i.e. Gonfolite Fm.; Oligocene time), passing upward to sandy marls (Marnoso-arenacea Fm.; Langhian to Messinian time), clays (i.e. Colombacci fm.; Messinian time), and evaporitic deposits (i.e. Gessoso Solifera fm.; Messinian time). The upper cycle, fed by both the northern Apennines and the southern Alps, mainly consists of marine sandy and conglomeratic formations (e.g. Sergnano Gravel,

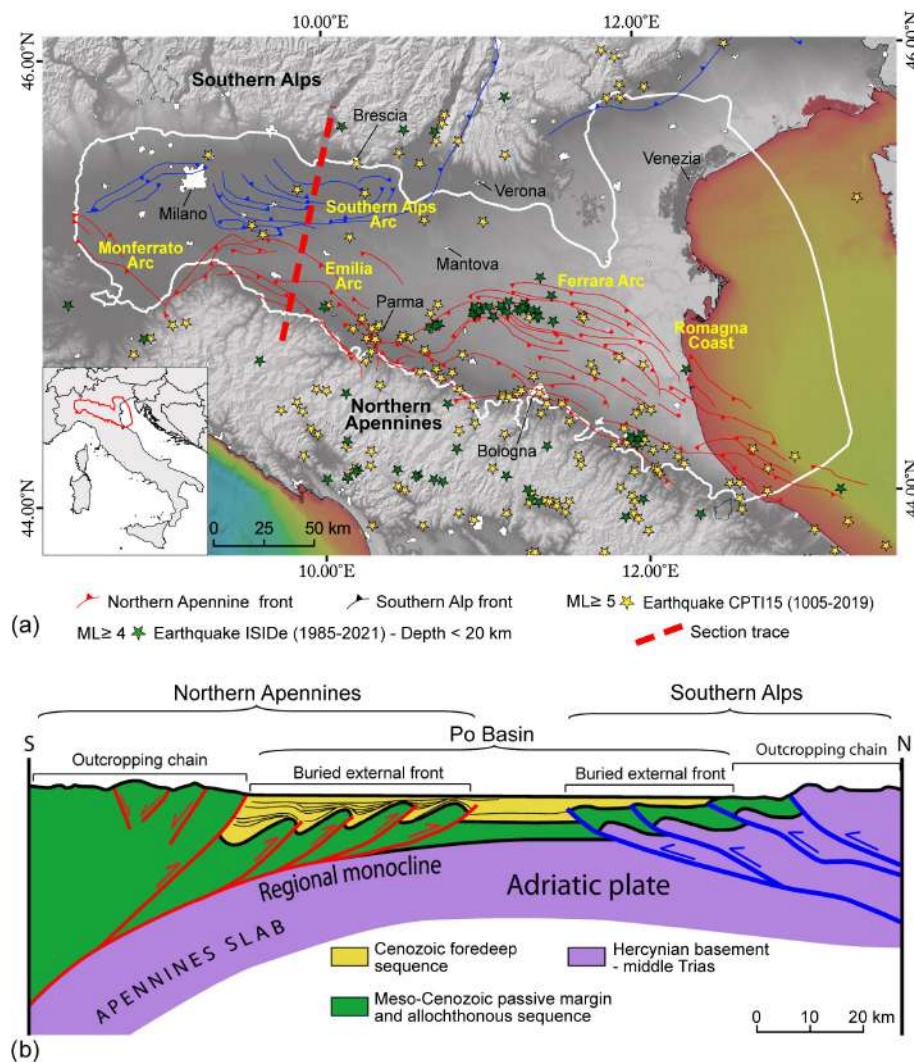


Figure 2. Study area and structural geology of the Po Plain. **(a)** Simplified structural map of the Po Plain (modified after Livani et al., 2018). The main buried thrusts of the northern Apennines (red colour) and southern Alps (blue colour) fronts are shown along with the instrumental and historical seismicity (ISIDe Working Group, 2010; Roviola et al., 2022). The white polygon represents the study area. **(b)** Schematic geological cross-section across the Po Plain along a N–S-oriented line (by Livani et al., 2018). The northern Apennines (on the left) and southern Alps (on the right) fronts can be identified under the Plio–Pleistocene sedimentary cover (in yellow) filling the Po Plain foredeep. Section trace is reported with a dashed red line in panel (a).

Porto Corsini, Porto Garibaldi, Santeramo, and Asti sandstones; Pliocene to middle–late Pleistocene time) and alluvial deposits (middle–late Pleistocene to present; e.g. Muttoni et al., 2003; Garzanti et al., 2011; Ghielmi et al., 2010, 2013; Livani et al., 2018). South of the Po River, the continental deposits consist of alluvial fan and plain deposits embedded in clays and showing elongated shapes, whereas, to the north of the Po River, the sedimentary bodies are wider, generally tabular, and with minor amounts of fine-grained sediments (Ori, 1993; Amorosi and Milli, 2001). These clastic sequences are superimposed on a carbonate and marly substratum (Triassic–middle Eocene), which lies on top of the platform and continental Permian–Triassic formations, lying

in turn on the Variscan crystalline basement (for more details about the carbonate sequence, refer to Livani et al., 2018, and references therein). The Triassic deposits are sometimes interposed by intra-sedimentary volcanic bodies (e.g. Pieri and Groppi, 1981; Castellarin, 1985; Cassano et al., 1986; Ghielmi et al., 2010; Livani et al., 2018). The southern Alps buried front consists of a repetition of Cenozoic clastic units stacked above a regional detachment in the Marne di Gallare Fm. (late Eocene) and followed at depth by deep thrust cutting the Mesozoic carbonates and the Variscan crystalline basement (Fantoni et al., 2004; Figs. 2b and 3). The northern Apennine chain developed by off-scraping the Meso–Cenozoic sedimentary cover of the subducting Adria plate

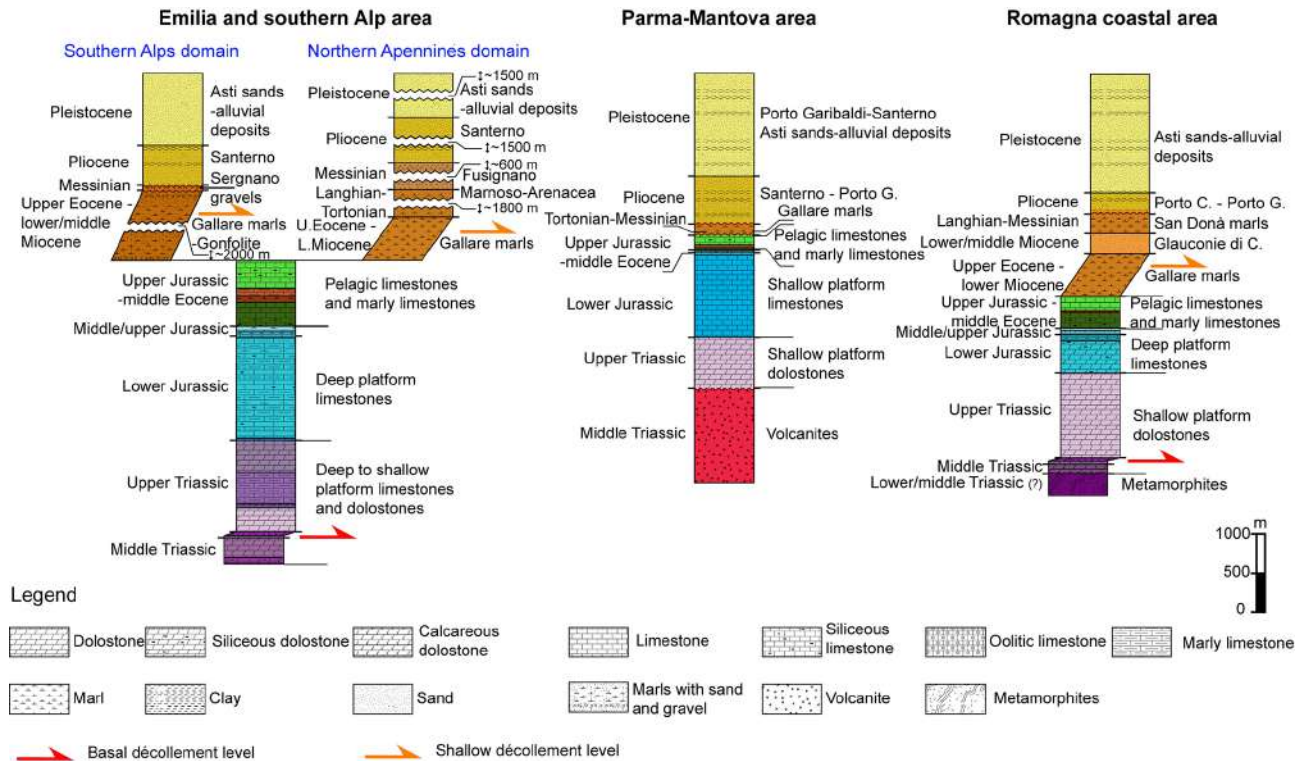


Figure 3. Synthetic stratigraphic columns of the Po Plain. From left to right: the stratigraphy of Emilia and the southern Alps, Parma-Mantova, and Romagna coastal areas is shown (see Fig. 2a). Sequences of the carbonate passive margin (from violet to green colours) and silicoclastic active margin (from brown to light-yellow colours) are distinguished. The main décollement levels are highlighted (red for basal décollement and orange for shallow décollement). The stratigraphic column to the left shows the different fillings and the different formation thicknesses of the southern Alps and the northern Apennines foredeep.

made up of siliciclastic, evaporitic, and shallow- to deep-water carbonate deposits (Cati et al., 1987; Bertotti et al., 1993; Casero et al., 1990; Zappaterra, 1990; Grandić et al., 2002; Fantoni and Scotti, 2003; Fantoni and Franciosi, 2010; Masetti et al., 2012; Fig. 3).

Due to the Apennine compressional deformation, the northern Apennines thrust system migrated toward the foreland over time (among many others, see Malinverno and Ryan, 1986; Doglioni, 1991; Patacca et al., 1990; Royden, 1988; Faccenna et al., 2003; Rosenbaum and Lister, 2004; Scrocca et al., 2006, 2007; Carminati and Doglioni, 2012, and references therein). The convergence is still active, as indicated by the moderate-to-high seismicity which historically affects the Po Plain (maximum M_w between 5.5 and 6.5; Rovida et al., 2020, 2022). Studies on the active stress field in Italy (Montone et al., 2004; Devoti et al., 2008; Cufaro et al., 2010; Montone et al., 2012), based on the analysis of earthquake focal mechanisms, GPS records, and borehole breakout data, identify active compression in the shallow portion of the Po Plain, with the maximum shortening axis being orthogonal to the main orogenic structures (i.e. NNE–SSW). Locally, the young land morphologies, the presence of different orders of fluvial terraces, and the deviation of some rivers

(including the Po River) near the buried active tectonic structures are the tangible evidence of the recent tectonic activity (e.g. Burrato et al., 1999, 2003; Boccaletti et al., 2004a, b; Wilson et al., 2009; Livio et al., 2009; Zuffetti and Bersezio, 2020; Bresciani and Perotti, 2014).

3 Database description

We realized our database by collecting, revising, and digitizing geological and geophysical data, originally in raster format, derived from public sources (i.e. databases and literature works). We collected 160 deep-well composite logs, 61 published geological cross-sections, and 10 geological maps (Fig. 4; Tables 1–3). The data were georeferenced to a common geographical system (WGS 84/UTM zone 32N; EPSG: 32632) by using the open-source QGIS software (version 3.16.7; <http://www.qgis.org>, last access: 15 May 2021) and were then uploaded into a 3D geological modelling software (Petrel® Software, version 2016.2). We organized the database into two groups, namely primitive data and derived data, containing further hierarchical subdivisions created for better organization and comprehension of the database.

Table 1. List and type of data collected for each lithological boundary.

Lithological boundary	Data source	Data type
Base of recent continental deposits	ViDEPI Project (2009–2023)	Well tops
	Boccaletti et al. (2011)	Geological cross-sections
	ISPRA (2015)	Geological cross-sections
	ISPRA (2015)	Isobath map
	Picotti et al. (2007)	Geological cross-sections
	Scardia et al. (2012)	Isobath map
	Wilson et al. (2009)	Geological cross-sections
Calabrian base	Wilson et al. (2009)	Geological cross-sections
	ViDEPI Project (2009–2023)	Well tops
	Boccaletti et al. (2011)	Geological cross-sections
	Casero (2004)	Geological cross-sections
	Cassano et al. (1986)	Geological cross-sections
	Fantoni and Franciosi (2009)	Geological cross-sections
	ISPRA (2015)	Geological cross-sections
	ISPRA (2015)	Isobath map
	Lindquist (1999)	Geological cross-sections
	Livani et al. (2018)	Geological cross-sections
	Maesano et al. (2015)	Geological cross-sections
	Picotti et al. (2007)	Geological cross-sections
	Pola et al. (2014)	Geological cross-sections
	Toscani et al. (2009)	Geological cross-sections
Pliocene base	Turrini et al. (2015)	Geological cross-sections
	Wilson et al. (2009)	Geological cross-sections
	ViDEPI Project (2009–2023)	Well tops
	Bigi et al. (1990a, b)	Isobath map
	Boccaletti et al. (2011)	Geological cross-sections
	Casero (2004)	Geological cross-sections
	Cassano et al. (1986)	Geological cross-sections
	Fantoni and Franciosi (2009)	Geological cross-sections
	ISPRA (2015)	Geological cross-sections
	ISPRA (2015)	Isobath map
	Livani et al. (2018)	Geological cross-sections
	Maesano et al. (2015)	Geological cross-sections
	Picotti et al. (2007)	Geological cross-sections
	Pola et al. (2014)	Geological cross-sections
Carbonate top	Toscani et al. (2009)	Geological cross-sections
	Turrini et al. (2015)	Geological cross-sections
	Wilson et al. (2009)	Geological cross-sections
	ViDEPI Project (2009–2023)	Well tops
	Boccaletti et al. (2011)	Geological cross-sections
	Casero (2004)	Geological cross-sections
	Casero et al. (1990)	Isobath map
	Cassano et al. (1986)	Geological cross-sections
	Fantoni and Franciosi (2009)	Geological cross-sections
	D'Ambrogio et al. (2023)	Isobath map
	ISPRA (2015)	Geological cross-sections
	ISPRA (2015)	Isobath map
	Lindquist (1999)	Geological cross-sections
	Livani et al. (2018)	Geological cross-sections
Magnetic basement top	Maesano et al. (2015)	Geological cross-sections
	Nicolich et al. (2004)	Isobath map
	Picotti et al. (2007)	Geological cross-sections
	Pola et al. (2014)	Geological cross-sections
	Toscani et al. (2009)	Geological cross-sections
	Turrini et al. (2015)	Geological cross-sections
	Wilson et al. (2009)	Geological cross-sections

Table 2. List of the geological cross-sections collected and used to build the 3D geological model. “Section number” refers to section traces reported in Fig. 4. “Figure number” refers to the figure in the original work. “Section” refers to the number of the section in the corresponding figure of the original work. “Repositioned” indicates whether the section trace has been modified according to the intersections with data located more accurately. “Section length” represents the length in kilometres of each geological sections. The total length of the collected geological cross-sections is 6341 km.

Section number (present work)	Data source	Figure number (source work)	Section (source work)	Repositioned	Section length (km)
1	Boccaletti et al., 2011	Fig. 5	A–A′		92.54
2		Fig. 5	B–B′	✓	59.3
3		Fig. 5	C–C′		50.6
4		Fig. 5	D–D′	✓	115.35
5		Fig. 5	E–E′	✓	53.16
6		Fig. 5	F–F′	✓	63.46
7		Fig. 5	G–G′		108.46
8		Fig. 5	H–H′		102.31
9		Fig. 5	H′–H′′		88.82
10	Casero (2004)	Plate 2	2a		46.11
11		Plate 3	3b	✓	97.24
12	Cassano et al. (1986)		3	✓	123.3
13			4	✓	131.36
14			5	✓	180.45
15			6	✓	103.58
16			7	✓	99.01
17			8	✓	106.33
18			9	✓	205.48
19			10	✓	279.5
20			11	✓	289.43
21			12	✓	351.38
22			13	✓	267.05
23	Fantoni and Franciosi (2009)	Fig. 3	1(1)	✓	30.94
24		Fig. 3	1(2)	✓	96.03
25		Fig. 3	2(1)	✓	86.48
26		Fig. 3	2(2)	✓	21.54
27		Fig. 3	3(1)	✓	42.23
28		Fig. 3	3(2)	✓	61.17
29		Fig. 3	3(3)	✓	48.03
30		Fig. 3	4	✓	92.45
31		Fig. 3	4	✓	98.25
32		Fig. 3	4	✓	131.64
33		Fig. 3	5	✓	238.39
34	ISPRA (2015)		A–A′		54.11
35			B–B′		57.99
36			C–C′		52.23
37	Lindquist (1999)	Fig. 3a		✓	117.06
38		Fig. 3b		✓	194.67
39		Fig. 3c			131.08
40	Livani et al. (2018)	Fig. 11	C–C′		62.4
41		Fig. 11	D–D′		58.78
42	Maesano et al. (2015)	Fig. 6	1		60.47
43		Fig. 6	2		78.36
44		Fig. 6	3		99.78
45		Fig. 6	4		84.22
46	Picotti et al. (2007)	Fig. 5	A–A′		140.53

Table 2. Continued.

Section number (present work)	Data source	Figure number (source work)	Section (source work)	Repositioned	Section length (km)
47	Pola et al. (2014)	Fig. 5	A–A'		27.72
48		Fig. 5	AA–AA'(1)		14.55
49		Fig. 5	AA–AA'(2)		20.09
50		Fig. 5	B–B'(1)		18.13
51		Fig. 5	B–B'(2)		8.21
52		Fig. 5	C–C'		27.35
53		Fig. 5	CC–CC'		29.90
54		Fig. 5	D–D'		21.10
55		Fig. 5	E–E'		22.26
56	Toscani et al. (2009)	Fig. 3	A–A'	✓	67.89
57		Fig. 3	B–B'	✓	67.74
58	Turrini et al. (2015)	Fig. 7	B		235.47
59		Fig. 7	C	✓	244.71
60		Fig. 7	D	✓	288.34
61	Wilson et al. (2009)	Fig. 2c		✓	94.82
Total length (km)					6341.33

The primitive data contain the product of the digitization of the collected isobath maps, the geological cross-sections, and the well data realized and acquired over a long period and for different purposes. The well data include specific sets of well logs aimed at the geological and/or mechanical characterization of the geological units. Therefore, to achieve the integration of the different sets of data, we analysed them with a focus on the stratigraphy and geological age of the interpreted units. Notice that, in 2009, the Executive Committee of the International Union of Geological Sciences (IUGS) ratified a new subdivision of the Quaternary Period and the Pleistocene Epoch, lowering the age of their base from the top of the Gelasian (1.8 Ma) to its base (2.58 Ma; Gibbard et al., 2010). Most of the collected data (Fig. 4; Tables 1, 2) refer to the pre-2009 chronostratigraphic subdivision including the Gelasian age in the upper Pliocene (Rio et al., 1998). On the contrary, some recent works reinterpreted the sedimentary sequence in the Po Plain and the nearby northern Adriatic Sea (e.g. Ghielmi et al., 2010, 2013; ISPRA, 2015; Maesano and D'Ambrogi, 2016; Amadori et al., 2019) using the new chronostratigraphic subdivision. In our database, since the collected primitive data (Fig. 4; Tables 1, 2) are both prior and successive to the 2009 chronostratigraphic subdivision, we homogenized the data considering the pre-2009 Pleistocene base as the Calabrian base.

We performed an accuracy analysis on the primitive data that unravelled several discrepancies in the interpretation of the subsurface geological horizons. Starting from these observations and considering the well data as the best constraint, we filtered the primitive isobath maps and the geological cross-sections to obtain a coherent dataset. The de-

rived data consist of these filtered isobath maps and the geological cross-sections plus a series of regional surfaces of the main geological units of the Po Plain subsurface. These surfaces were generated without considering the fault occurrences and/or displacements, and they were gridded by means of interpolation of filtered primitive data.

All data (both primitive and derived) are provided in a delimited text file format and are organized according to the data type (i.e. well, geological cross-section, map, or gridded surface).

During the processes of data collection and revision, some published subsurface data reconstructions might not have been included in the database for technical reasons, such as isobath maps being published at an inappropriate resolution, depth contour lines not being properly stated, or geological cross-sections having a different lithostratigraphic and structural scheme compared to the one used in this work.

Figure 5 summarizes the technical procedures and the workflow used to process the data and to develop the database. In the following paragraphs, the methods and the produced primitive data are explained in detail.

4 Primitive data: methods and results

Primitive data derive from the digitization of public data that have been graphically and spatially checked to eliminate errors due to low graphical quality and distortions, scale errors, or bad positioning. We digitized the principal horizons reported in the geological cross-sections; the isobaths of the main geological surfaces represented in the geological maps; and the well locations, comprised of their trajectory

Table 3. Wells collected in the database with their location (x coordinate and y coordinate) and the rotary table elevation (m a.s.l.). The coordinates of wellhead locations are reported in the geographical system used in the database (WGS 84/UTM zone 32N; EPSG: 32632). UOI: well identification number. The deepest lithology unit reached by each well corresponds to the following: (1) recent continental deposits, (2) late Pliocene–Pleistocene deposits, (3) late Miocene–late Pliocene deposits, (4) early–late Miocene deposits, (5) Triassic–Eocene carbonate units, and (6) crystalline basement.

UOI	Well name	x (well head)	y (well head)	Rotary table (m a.s.l.)	Deepest lithology unit
W001	Adele 1	775896	4948539	26.0	3
W002	Adriana 1	813510	4935428	26.0	4
W003	Afrodite 1	776447	4949455	17.5	4
W004	Agnadello 1	540028	5032805	101.0	4
W005	Albertina 1	817436	4975718	12.5	4
W006	Alex 1	814736	4925902	22.0	4
W007	Alma 1	811808	4913895	12.2	3
W008	Amelia 2Bis	797531	4917463	21.2	3
W009	Anguilla 1	782121	4910090	18.3	3
W010	Antegnate 1	562955	5037036	114.0	4
W011	Antinea 1Bis	796791	4889359	18.9	5
W012	Arcade 1	750637	5073687	65.0	5
W013	Arcobaleno 1	776213	5018899	23.4	4
W014	Arese 1	504947	5044530	170.2	4
W015	Arlecchino 1	779266	5013094	24.7	4
W016	Arluno 1	495098	5038326	155.5	4
W017	Azzura 1	784981	4941745	27.0	3
W018	Baggiovara 1	645422	4940921	65.2	4
W019	Ballan 1	735056	5044275	21.4	5
W020	Bando 7	725514	4949472	5.0	4
W021	Baricella 1	702411	4949324	12.2	3
W022	Baura 001	714740	4971856	9.4	4
W023	Bedeschi 1 dir	727384	4922999	21.0	4
W024	Bedeschi 1 dirA	727384	4922999	21.0	4
W025	Belgoioso 1	523877	4998221	79.0	4
W026	Bellaria Mare 1	780580	4894982	17.6	4
W027	Berillo 1	786889	4908968	18.9	3
W028	Bertolani 1 Dir	640133	4940818	79.0	4
W029	Bevilacqua 1	677149	4958950	19.3	3
W030	Bosco Rosso 1	616314	4975044	32.5	3
W031	Brignano 2	551050	5046463	157.0	5
W032	Canopo 1	796699	4884893	19.0	5
W033	Cantoni 1	603577	4987473	36.0	4
W034	Cagnacco 1	827970	5102613	87.0	6
W035	Carmela 1	866844	4895571	27.0	2
W036	Cascina Buzzoni 1	723577	4967057	9.0	4
W037	Cascina Nuova 1 dir	701791	4976442	16.0	5
W038	Cascina San Francesco 1	737689	4963897	4.5	4
W039	Cascina San Pietro 1 dir	542559	5032244	100.0	4
W040	Case Pinelli 1	657445	4950268	34.7	4
W041	Casello 1 dir	593907	4970938	48.0	4
W042	Castano 1	481511	5043078	182.4	5
W043	Castel Gabbiano 1	557324	5036392	108.0	4
W044	Cerere 1	802948	4927606	26.0	3
W045	Cernusco 1	527759	5040908	136.0	4
W046	Cernusco 3	527060	5037627	123.0	4
W047	Chiosone 1	570184	4999305	45.8	4
W048	Cinzia 1	835893	4909975	26.0	4
W049	Claudia 1	822486	4954196	27.5	4
W050	Codevigo 1	741986	5014848	5.0	5
W051	Cona 2	709424	4964097	8.2	4
W052	Cornegliano 19	532686	5013752	89.0	4

Table 3. Continued.

UOI	Well name	x (well head)	y (well head)	Rotary table (m a.s.l.)	Deepest lithology unit
W053	Correggio 33	636767	4957061	41.8	3
W054	Correggio 34 dir	637237	4960570	39.0	3
W055	Correggio 35 dir	637233	4960569	39.0	3
W056	Correggio 36 dir	637231	4960569	39.0	3
W057	Correggio 37 dir	637229	4960566	39.0	3
W058	Correggio 38 dir	637224	4960564	39.0	3
W059	Correggio 39 dir	637222	4960562	39.0	3
W060	Correggio 39 dirA	637222	4960562	39.0	3
W061	Correggio 40 dir	635457	4958855	41.0	3
W062	Corsico 1	506882	5029271	115.4	4
W063	Corte Mezzo 1	739452	4960575	6.0	3
W064	Corte Vittoria 1	735863	4976384	10.0	5
W065	Cusignana 1	745549	5073487	80.0	5
W066	Daniela 1	791415	4972060	25.0	4
W067	Dolo 1 dir	740530	5031608	8.0	3
W068	Fabbrico 1	644606	4971873	23.5	3
W069	Ferrara 1	714006	4965211	13.0	5
W070	Filetto 1	745087	4912388	18.0	4
W071	Filetto 1 dirA	745087	4912388	18.0	4
W072	Gallignano 2	563219	5030619	93.0	4
W073	Gandini 2 dir	544340	5029732	96.7	3
W074	Gemma 1	830405	4912198	27.5	4
W075	Ghiara 2 dir	593461	4969928	51.0	4
W076	Ginevra 1	782492	4939951	26.0	3
W077	Gisolo 1	580476	4959830	285.0	4
W078	Gladiolo 1	811922	4958195	27.0	4
W079	Glenda 1	825659	4949631	27.0	4
W080	Goro 1	761932	4974041	7.0	4
W081	Gudo Gambaredo 1 dir	509669	5025876	111.0	2
W082	Inverno 1dir	530799	5005318	84.1	4
W083	Irma 1	794204	4961737	27.0	4
W084	Isabella 1	811951	4985391	27.4	4
W085	Lanzano 1	529337	5026512	96.9	4
W086	Linarolo 1	522494	5000129	86.0	4
W087	Locate Triulzi 1	517074	5022007	103.6	3
W088	Maiero 1	727422	4956521	6.5	4
W089	Malossa 4	542687	5041078	130.4	5
W090	Malossa B Iniezione	544749	5039426	130.0	4
W091	Mariangela 1	779126	4994676	26.0	3
W092	Marrara 1	706920	4955104	18.7	4
W093	Marzeno 41	729689	4900222	177.0	5
W094	Merlengo 1	746589	5066132	48.2	4
W095	Mirazzano 1 dir	525371	5033901	114.0	3
W096	Molinella 1	710103	4946510	15.0	4
W097	Montalbano 21	704740	4954756	11.2	4
W098	Monte Acuto 1 dir	532837	4991334	79.0	4
W099	Montecchi 1	629875	4943513	101.8	4
W100	Montecchio 1	720948	4977826	8.0	4
W101	Moretta 1	385425	4956518	269.2	6
W102	Muradolo 1	565668	4988208	48.0	4
W103	Negrini 1	726897	4942291	4.2	4
W104	Nervesa 1	752475	5076899	73.5	5
W105	Nervesa 1 dirA	752475	5076899	73.5	4
W106	Novi Ligure 2	485442	4956778	192.5	3
W107	Offanengo 1	557914	5026164	86.0	3
W108	Oriana 1	827485	4916892	26.0	4

Table 3. Continued.

UOI	Well name	x (well head)	y (well head)	Rotary table (m a.s.l.)	Deepest lithology unit
W109	Ornella 1	787040	4975930	18.9	4
W110	Paese 1 dir	743131	5062880	39.0	4
W111	Pandino 1	536388	5029141	87.0	4
W112	Pavonara 1	711695	4973319	8.0	4
W113	Portoverrara 3	727680	4952637	4.6	4
W114	Priorato 1	592876	4969565	50.0	4
W115	Priorato 2 dir	592876	4969565	50.0	3
W116	Pumenengo 1	566508	5038091	123.0	4
W117	Quarto 1	552990	4982890	89.0	4
W118	Rachele 1	805089	5020241	27.0	4
W119	Raffaella 2	804262	4968628	27.6	4
W120	Rea 1 dir	512307	4994494	73.0	5
W121	Riccardina 1	701174	4938999	25.9	4
W122	Rolassa 1	440470	4975679	156.0	4
W123	Russi 1 dir	742428	4915614	15.0	4
W124	Salerano 001	530085	5015436	83.4	4
W125	San Alessandro 1	596519	4968724	55.0	4
W126	San Alessandro 1 dirA	596519	4968724	55.0	3
W127	San Cipriano 1	545609	5019541	72.9	3
W128	San Ermelinda 1	729376	4945094	2.0	3
W129	San Genesio 1	515135	5008502	95.5	5
W130	San Michele 1	596263	4947217	241.0	4
W131	San Polo 1 dir	556581	4981094	93.0	4
W132	Sartirana 1	473042	4994514	108.0	4
W133	Scandiano 1 dirB	637657	4941105	80.2	4
W134	Scandiano 2 dir	639189	4940924	75.2	4
W135	Schiorsi 1	733784	4955454	4.3	3
W136	Segrate 1	522534	5037547	122.0	4
W137	Seniga 1	591646	5012369	56.0	3
W138	Serena 1	816551	4890738	28.6	3
W139	Seresole 1	546169	5035239	112.0	4
W140	Sermide 1	684777	4983402	16.9	3
W141	Settimo Milanese 1	503716	5035857	146.5	5
W142	Solarolo 1	606267	4993664	43.0	5
W143	Sommariva Del Bosco 1	403848	4959735	307.7	4
W144	Spada 1	682501	4959755	24.9	4
W145	Torrazza 1	762257	4918726	6.0	2
W146	Torre Del Poggio 1	550408	4986992	75.0	4
W147	Torrente Riglio 1 dir	564192	4983772	66.0	4
W148	Trava 1	739883	4952560	3.2	3
W149	Trenno 1	506511	5037331	146.0	4
W150	Trescore 1	550917	5028054	86.4	4
W151	Urago D'Oglio 1	568054	5040092	121.0	4
W152	Vaiano 1	535573	5033071	104.3	4
W153	Valgera 1	439138	4975331	131.0	4
W154	Valle Isola 1	753080	4956134	8.0	3
W155	Valletta 1 dir	712816	4935159	15.0	3
W156	Varano 1	746924	4964965	8.5	4
W157	Vigatto 10 dir	602968	4952521	132.2	4
W158	Vignola 1	717279	4977064	11.5	5
W159	Villavecchia 1 dir	591224	4950301	237.2	4
W160	Zoboli 1	648649	4938952	70.0	4

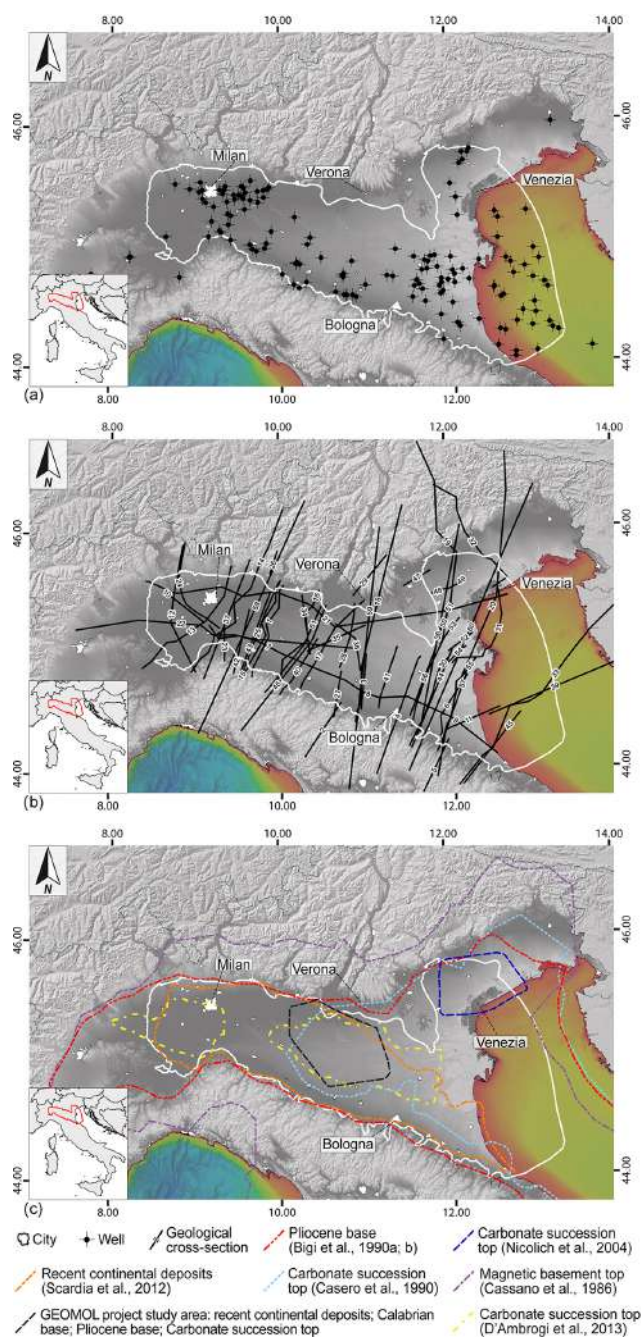


Figure 4. Primitive data collected from public sources (i.e. databases and articles from the literature). **(a)** Geographical locations of the 160 wells from which well data were collected and digitized. Some areas of the Po Plain are characterized by a low well density, hence the successive primitive data collection (i.e. geological cross-sections and maps) was focused within a slightly reduced area indicated by the white polygon. **(b)** Traces of the geological cross-sections collected from the literature (the number on each section corresponds to a specific geological cross-section in Table 1 where the data source is specified). **(c)** Primitive data from geological subsurface maps. The source is reported in the legend.

along depth, lithological and stratigraphical information, and geophysical logs from well composite logs. We performed the entire workflow (data collection, image georeferencing, data quality check, integration, and model building) by using QGIS and Petrel[®] software. The digitized data were then organized into text files. Further details about the data processing are given below.

4.1 Well data

The source of well data is the ViDEPI project database (<http://www.videpi.com>, last access: 1 July 2023). We collected data from 160 well logs, originally in a raster format (scale 1 : 1000), drilled in the Po Plain and in the northern Adriatic Sea (Fig. 4). Borehole information, such as wellhead coordinates, rotary table elevation, measured depths, true depths, total depth, and deviation survey, is indicated on the composite logs, along with lithological, stratigraphic, and fluid saturation information (Fig. 6). In addition, composite logs include the spontaneous potential log (SP), which is used for lithological characterization and stratigraphic correlation purposes, and the resistivity log (Res), which is used for the identification of hydrocarbon-bearing intervals; in the more recent well master logs, the SP log is replaced by, or in certain cases complemented by, a gamma ray log (GR). Furthermore, 133 out of 160 well composite logs of our dataset also include sonic log registrations that provide insights into sonic velocity variations with depth (Fig. 6). Further lithological information derives either from drill cuttings or from laboratory analysis of core samples collected from wells.

An accurate revision of the wellhead positioning and the subsurface trajectory was necessary to properly collect and organize the well data and to furnish a dataset suitable to be imported into the most common 3D modelling software. From each well, we first transformed the reported geographic coordinates (expressed in ROMA 40 as geodetic datum) into projected coordinates using the WEST BOAGA projection (geodetic datum: ROMA 40) and then converted into the geographical system used for our database (i.e. WGS 84/UTM zone 32N; EPSG: 32632). Most of the wells are vertical; hence, the well trajectory at depth is set using the wellhead coordinates and the total depth values. On the contrary, the path of the directional wells was reconstructed by using inclination (Inc) and azimuth (Az) information at the depth reported in the composite logs.

We then digitized the available SP log, GR log, and sonic log of each well using the WebPlotDigitizer software (Rohatgi, 2014). Table 4 shows the log availability for each well in the project. The digitization procedure was performed manually with a variable sampling step or by means of a semi-automatic method of line recognition. The digitized logs were then resampled to a constant step of 0.5 m. Figure 7 shows an example of the digitization process.

The resistivity log (Res) was used to identify the mineralized intervals of wells with gas-bearing layers and then to

Table 4. List of collected wells and the relative log availability. “UOI” indicates the identification number for each well. GR: gamma ray log. SP: spontaneous potential log.

UOI	Well name	GR	Lithology	Mineralization	Sonic	SP
W001	Adele 1		✓	✓	✓	✓
W002	Adriana 1		✓	✓	✓	✓
W003	Afrodite 1		✓	✓	✓	✓
W004	Agnadello 1		✓	✓		✓
W005	Albertina 1		✓	✓	✓	✓
W006	Alex 1		✓	✓		✓
W007	Alma 1		✓	✓		✓
W008	Amelia 2Bis		✓	✓		✓
W009	Anguilla 1		✓	✓	✓	✓
W010	Antegnate 1		✓	✓		✓
W011	Antinea 1Bis		✓	✓		✓
W012	Arcade 1		✓	✓	✓	✓
W013	Arcobaleno 1	✓	✓	✓	✓	
W014	Arese 1		✓	✓		✓
W015	Arlecchino 1	✓	✓	✓	✓	
W016	Arluno 1		✓	✓		✓
W017	Azzura 1		✓	✓	✓	✓
W018	Baggiovara 1		✓	✓	✓	✓
W019	Ballan 1	✓	✓	✓	✓	
W020	Bando 7		✓	✓	✓	✓
W021	Baricella 1		✓	✓		✓
W022	Baura 001		✓	✓		✓
W023	Bedeschi 1 dir		✓	✓	✓	✓
W024	Bedeschi 1 dirA		✓	✓	✓	✓
W025	Belgoioso 1		✓	✓	✓	✓
W026	Bellaria Mare 1		✓	✓		✓
W027	Berillo 1		✓	✓	✓	✓
W028	Bertolani 1 Dir		✓	✓	✓	✓
W029	Bevilacqua 1		✓	✓	✓	✓
W030	Bosco Rosso 1		✓	✓	✓	✓
W031	Brignano 2		✓	✓	✓	✓
W032	Canopo 1		✓	✓		✓
W033	Cantoni 1		✓	✓	✓	✓
W034	Cargnacco 1		✓	✓	✓	✓
W035	Carmela 1		✓	✓	✓	✓
W036	Cascina Buzzoni 1		✓	✓	✓	
W037	Cascina Nuova 1 dir		✓	✓	✓	✓
W038	Cascina San Francesco 1		✓	✓	✓	✓
W039	Cascina San Pietro 1 dir		✓	✓	✓	✓
W040	Case Pinelli 1		✓	✓	✓	✓
W041	Casello 1 dir	✓	✓	✓	✓	
W042	Castano 1	✓	✓	✓	✓	✓
W043	Castel Gabbiano 1		✓	✓	✓	✓
W044	Cerere 1		✓	✓	✓	✓
W045	Cernusco 1		✓	✓		✓
W046	Cernusco 3		✓	✓		✓
W047	Chiosone 1		✓	✓	✓	✓
W048	Cinzia 1		✓	✓	✓	✓
W049	Claudia 1		✓	✓	✓	✓
W050	Codevigo 1		✓	✓	✓	✓
W051	Cona 2		✓	✓		✓
W052	Cornegliano 19		✓	✓		✓
W053	Correggio 33		✓	✓	✓	✓
W054	Correggio 34 dir		✓	✓	✓	✓
W055	Correggio 35 dir		✓	✓	✓	✓

Table 4. Continued.

UOI	Well name	GR	Lithology	Mineralization	Sonic	SP
W056	Correggio 36 dir		✓	✓	✓	✓
W057	Correggio 37 dir		✓	✓	✓	✓
W058	Correggio 38 dir		✓	✓	✓	✓
W059	Correggio 39 dir		✓	✓	✓	✓
W060	Correggio 39 dirA		✓	✓	✓	✓
W061	Correggio 40 dir		✓	✓	✓	✓
W062	Corsico 1		✓	✓		✓
W063	Corte Mezzo 1		✓	✓	✓	✓
W064	Corte Vittoria 1	✓	✓	✓	✓	✓
W065	Cusignana 1		✓	✓	✓	✓
W066	Daniela 1		✓	✓	✓	✓
W067	Dolo 1 dir		✓	✓	✓	✓
W068	Fabbrico 1		✓	✓	✓	✓
W069	Ferrara 1		✓	✓		✓
W070	Filetto 1		✓	✓	✓	✓
W071	Filetto 1 dirA		✓	✓	✓	✓
W072	Gallignano 2		✓	✓		✓
W073	Gandini 2 dir		✓	✓	✓	✓
W074	Gemma 1		✓	✓	✓	✓
W075	Ghiara 2 dir		✓	✓	✓	✓
W076	Ginevra 1		✓	✓	✓	✓
W077	Gisolo 1		✓	✓	✓	✓
W078	Gladiolo 1		✓	✓	✓	✓
W079	Glenda 1		✓	✓	✓	✓
W080	Goro 1		✓	✓	✓	✓
W081	Gudo Gambaredo 1 dir		✓	✓	✓	✓
W082	Inverno 1dir		✓	✓	✓	
W083	Irma 1		✓	✓	✓	✓
W084	Isabella 1		✓	✓	✓	✓
W085	Lanzano 1		✓	✓		✓
W086	Linarolo 1		✓	✓	✓	✓
W087	Locate Triulzi 1		✓	✓		✓
W088	Maiero 1		✓	✓		✓
W089	Malossa 4	✓	✓	✓		✓
W090	Malossa B Iniezione		✓	✓	✓	✓
W091	Mariangela 1		✓	✓	✓	✓
W092	Marrara 1		✓	✓		✓
W093	Marzeno 41		✓	✓	✓	✓
W094	Merlengo 1	✓	✓	✓	✓	
W095	Mirazzano 1 dir		✓	✓	✓	✓
W096	Molinella 1		✓	✓	✓	✓
W097	Montalbano 21		✓	✓		✓
W098	Monte Acuto 1 dir		✓	✓	✓	✓
W099	Montecchi 1		✓	✓	✓	✓
W100	Montecchio 1		✓	✓	✓	✓
W101	Moretta 1		✓	✓	✓	✓
W102	Muradolo 1		✓	✓	✓	✓
W103	Negrini 1		✓	✓	✓	✓
W104	Nervesa 1	✓	✓	✓	✓	
W105	Nervesa 1 dirA	✓	✓	✓	✓	
W106	Novi Ligure 2		✓	✓	✓	✓
W107	Offanengo 1		✓	✓	✓	✓
W108	Oriana 1		✓	✓	✓	✓
W109	Ornella 1		✓	✓	✓	✓
W110	Paese 1 dir	✓	✓	✓	✓	
W111	Pandino 1		✓	✓		✓

Table 4. Continued.

UOI	Well name	GR	Lithology	Mineralization	Sonic	SP
W112	Pavonara 1		✓	✓	✓	✓
W113	Portoverrara 3		✓	✓		✓
W114	Priorato 1		✓	✓	✓	✓
W115	Priorato 2 dir		✓	✓	✓	✓
W116	Pumenengo 1		✓	✓	✓	✓
W117	Quarto 1	✓	✓	✓	✓	
W118	Rachele 1		✓	✓	✓	✓
W119	Raffaella 2		✓	✓	✓	✓
W120	Rea 1 dir		✓	✓	✓	✓
W121	Riccardina 1		✓	✓	✓	✓
W122	Rolassa 1		✓	✓	✓	✓
W123	Russi 1 dir		✓	✓	✓	✓
W124	Salerano 001		✓	✓		✓
W125	San Alessandro 1		✓	✓	✓	✓
W126	San Alessandro 1 dirA		✓	✓	✓	✓
W127	San Cipriano 1		✓	✓		✓
W128	San Ermelinda 1		✓	✓	✓	✓
W129	San Genesio 1	✓	✓	✓	✓	✓
W130	San Michele 1		✓	✓	✓	✓
W131	San Polo 1 dir		✓	✓	✓	✓
W132	Sartirana 1		✓	✓	✓	✓
W133	Scandiano 1 dirB		✓	✓	✓	✓
W134	Scandiano 2 dir		✓	✓	✓	✓
W135	Schiorsi 1		✓	✓	✓	✓
W136	Segrate 1		✓	✓		✓
W137	Seniga 1		✓	✓	✓	✓
W138	Serena 1		✓	✓	✓	✓
W139	Seresole 1		✓	✓	✓	✓
W140	Sermide 1		✓	✓	✓	✓
W141	Settimo Milanese 1		✓	✓	✓	✓
W142	Solarolo 1		✓	✓	✓	✓
W143	Sommariva Del Bosco 1	✓	✓	✓	✓	✓
W144	Spada 1		✓	✓		✓
W145	Torrazza 1	✓	✓	✓	✓	✓
W146	Torre Del Poggio 1		✓	✓	✓	✓
W147	Torrente Riglio 1 dir		✓	✓	✓	✓
W148	Trava 1		✓	✓	✓	
W149	Trenno 1	✓	✓	✓		✓
W150	Trescore 1		✓	✓		✓
W151	Urago D'Oglio 1		✓	✓	✓	✓
W152	Vaiano 1		✓	✓	✓	✓
W153	Valgera 1		✓	✓	✓	✓
W154	Valle Isola 1		✓	✓	✓	✓
W155	Valletta 1 dir		✓	✓	✓	✓
W156	Varano 1		✓	✓		✓
W157	Vigatto 10 dir		✓	✓	✓	✓
W158	Vignola 1		✓	✓	✓	✓
W159	Villavecchia 1 dir		✓	✓	✓	✓
W160	Zoboli 1		✓	✓	✓	✓

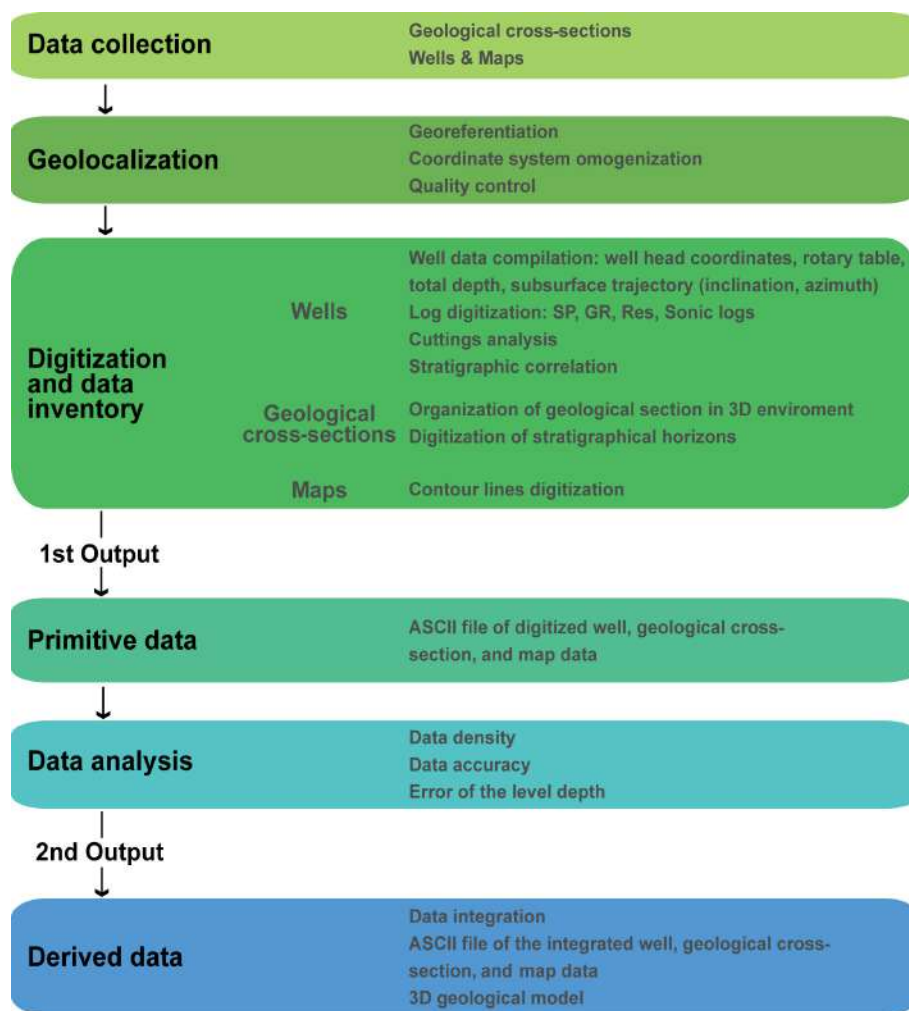


Figure 5. Workflow used for the database creation.

create a new discrete type of log with indications regarding hydrocarbon-bearing and water-bearing layers. Subsequently, Res was used to isolate and remove the sonic log measurements for those geological intervals affected by the hydrocarbon presence (Figs. 7 and 8).

The stratigraphic information on the composite logs together with the SP and GR logs was used to perform a correlation at the regional scale by identifying those units showing different lithological properties and defining surfaces dividing geological successions with different mechanical properties. The main units recognized are outlined (from youngest to oldest) as follows:

- recent clastic deposits of the Po Plain and the Adriatic Sea, consisting of gravels and sands of the continental environment identified from the cuttings of the first tens to hundreds of metres for each well – this unit has been widely analysed in the literature (Regione Emilia Romagna and Eni-AGIP, 1998; Regione Lombardia and

Eni-AGIP, 2002; Scardia et al., 2012; Ghielmi et al., 2013);

- late Pliocene–Pleistocene sand-rich sequences consisting of sands and clayey sands with clayey interlayers of deep-marine to continental environments (Sabbie di Asti Group), connected to the latest filling of the Po Plain foredeep;
- late Miocene–late Pliocene clastic deposits connected to the evolution of the northern Apennine foredeep and top-thrust basins, including
 - i. clay-rich units made up of variably silty clays with minor sand (Argille del Santerno Fm.)
 - ii. sand-rich (mostly foredeep turbiditic) units made up of thick sand beds with minor clay and thin-bedded sand–clay repetitions (e.g. Marnoso-Arenacea Fm., Bagnolo Fm., Fusignano Fm., Caviga Fm., Porto Garibaldi Fm., Porto Corsini Fm.)

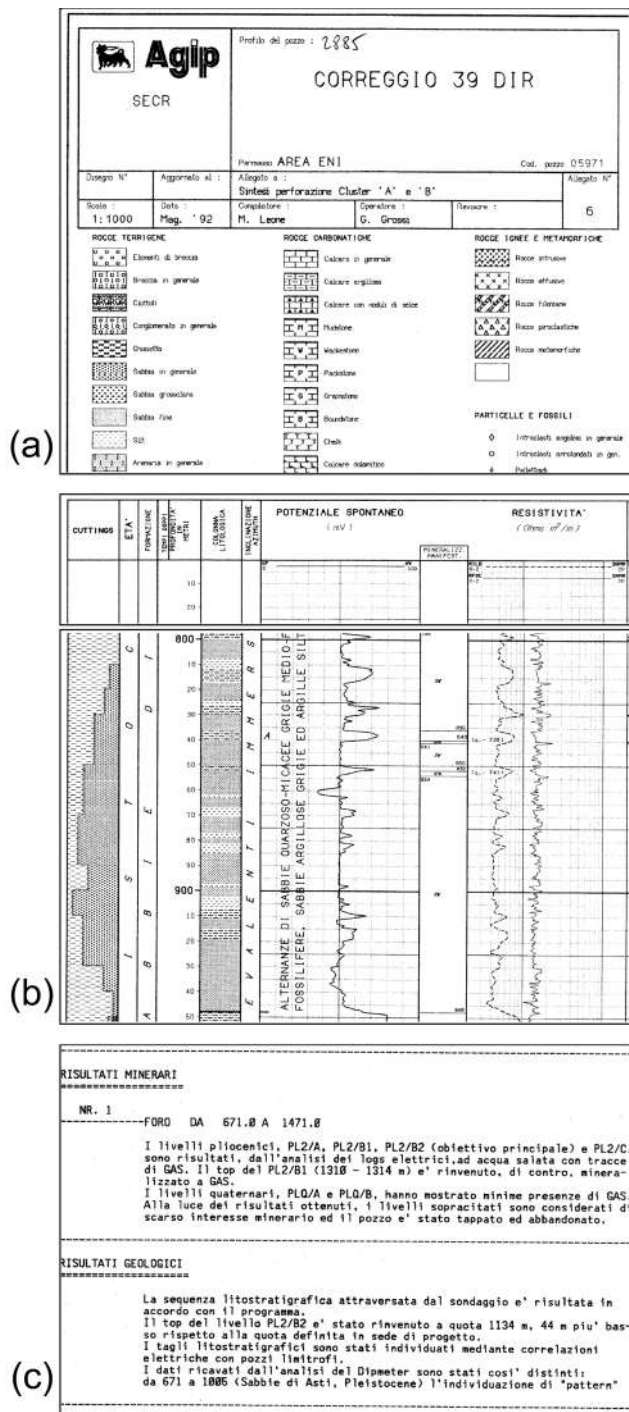


Figure 6. Typical composite log (scale 1 : 1000) available from the ViDEPI database (<http://www.videpi.com>, last access: 1 July 2023), originally in .pdf format. (a) Section of the well name, well coordinates information, and well log legend. (b) Section of the well log data, lithological cuttings, and completion information. (c) Notes section (e.g. well trajectory, core information, geological information, technical data).

iii. conglomeratic units made up of shallow-marine and fluvio-deltaic conglomerates and sands with minor clay (e.g. Sergnano Fm., Cortemaggiore Fm., Boreca Conglomerate);

- early-late Miocene marly sequences, consisting of marl, clayey marl, clay, and sandy marl with sand intercalations recording deposition on the foreland; ramp (e.g. Marne di Gallare Group)
- Triassic to Eocene undifferentiated carbonate units consisting of prevailing limestone (mainly mudstone and packstone–grainstone) and dolomite with subordinate marl;
- Variscan crystalline basement.

We collected additional data related to the lithological characteristics of the subsurface sedimentary units from cutting descriptions. The cutting descriptions contain the information collected during mud logging, where rock fragments from the borehole reach the surface due to the circulation of the drilling fluids. Those data were combined with the SP and GR logs and with lithological data from core sample analysis reported in the well profile to characterize the lithology of the entire well. In total, we identified nine macro-lithologies, which are listed below together with the descriptions commonly found in the well profiles:

- gravel (e.g. polygenic gravel, gravel prevalent, polygenic gravel and sand with shale interbeds, and gravel and pebbles with sand interbeds)
- sand (e.g. sand, sand prevalent, shaly sand, fine sand, sand with shale interbeds, sand and shaly sands, and sand banks)
- cemented sand (e.g. cemented sand, fine-grained cemented sand, cemented sand and pebbles, calcareous cemented sand, and sand of variable cementation)
- shale (e.g. shale, silty shale, grey shale, marl shale, and prevalent shale)
- sand and shale alternances (e.g. grey shales and sand and shales with sand interbeds)
- conglomerates (e.g. polygenic conglomerate, polygenic conglomerate with shale, and polygenic conglomerate with sand interbeds)
- marl (e.g. marls, silty marls, grey silty marls, marls and sandy marls, and grey marls with cemented sand)
- dolomite (e.g. dolomite, calcareous dolomite, crystalline dolomite, shaly dolomite, and grey dolomite)
- limestone (mudstone, wackestone, packstone, and grainstone).

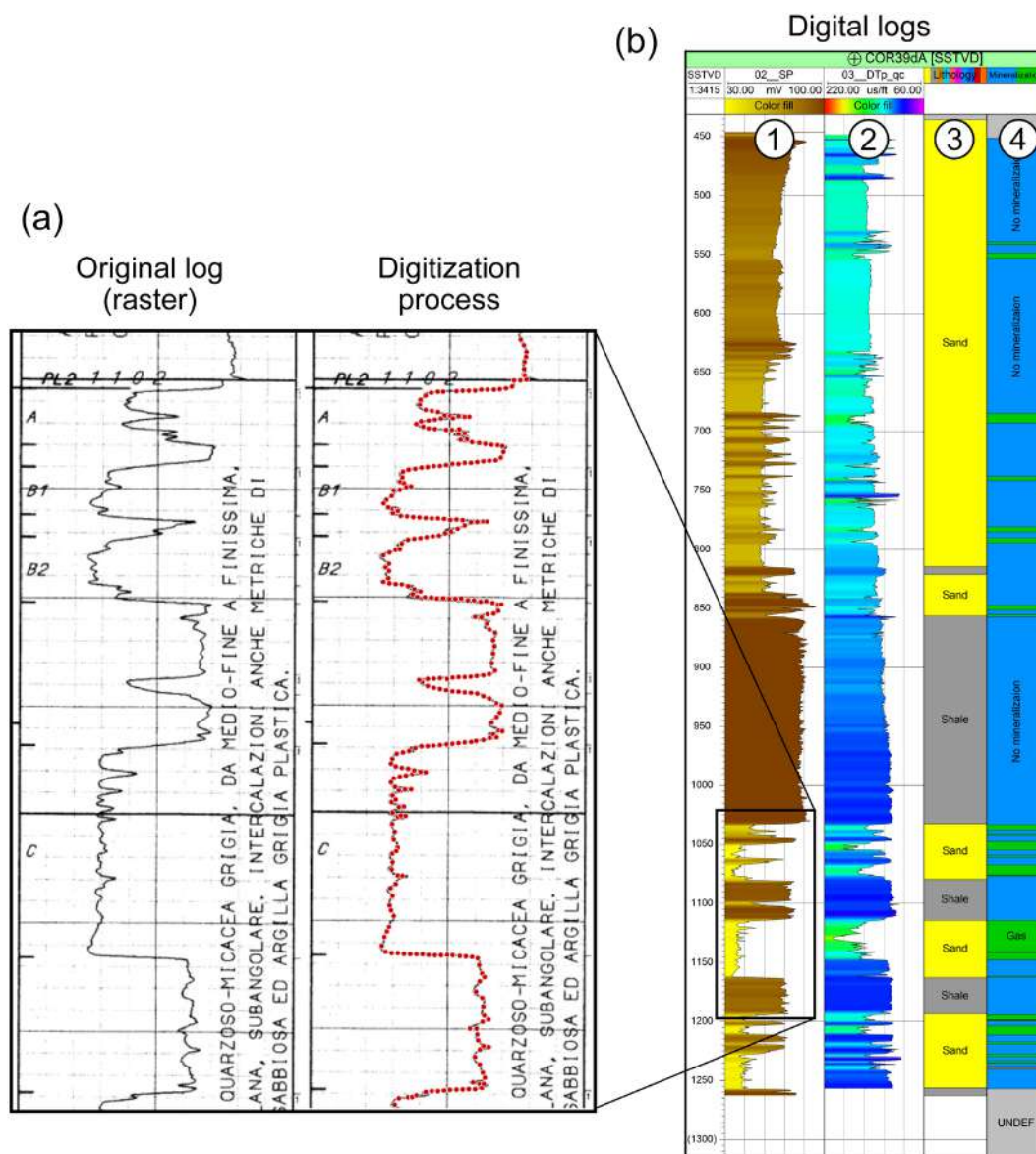


Figure 7. Example of the digitization process for well Correggio 39 dirA. Panel (a) shows the original spontaneous potential log in the composite log (raster format) and the digitalized points (in red). Panel (b) shows the digitized (1) SP and (2) sonic logs and the classification of (3) lithology and (4) hydrocarbon-bearing sections.

Well data represent the main constraint for the subsequent 3D geological modelling phase. As shown in Fig. 4, the distribution of the wells in the area is not homogeneous, and some regions are characterized by low well density. For this reason, the collection of the other primitive data (i.e. geological cross-sections and maps) was focused in the area indicated by the white polygon in Fig. 4, excluding the most isolated wells.

We performed a preliminary analysis of the sonic velocity variations with depth using the collected data and the newly created lithological and mineralization logs (Fig. 8). The sonic logs display transit time values in the range of 40–

140 $\mu\text{s ft}^{-1}$ (131–459 $\mu\text{s m}^{-1}$). However, we observed higher values (approx. 150–200 $\mu\text{s ft}^{-1}$ (492–656 $\mu\text{s m}^{-1}$)) concentrated to the first tens to a few hundred metres from the surface which are mostly connected to gravel lithologies characterized by poor consolidation (Fig. 8). In some cases, unusually high or low sonic log values with respect to the general data trend for a certain lithology can be ascribed to the presence of thin layers with different lithological characteristics, to possible borehole damage, or to the presence of fractures. The currently available information does not allow a clear interpretation of their causes and even their removal. Most of the lithologies show a gradual decrease in transit time with

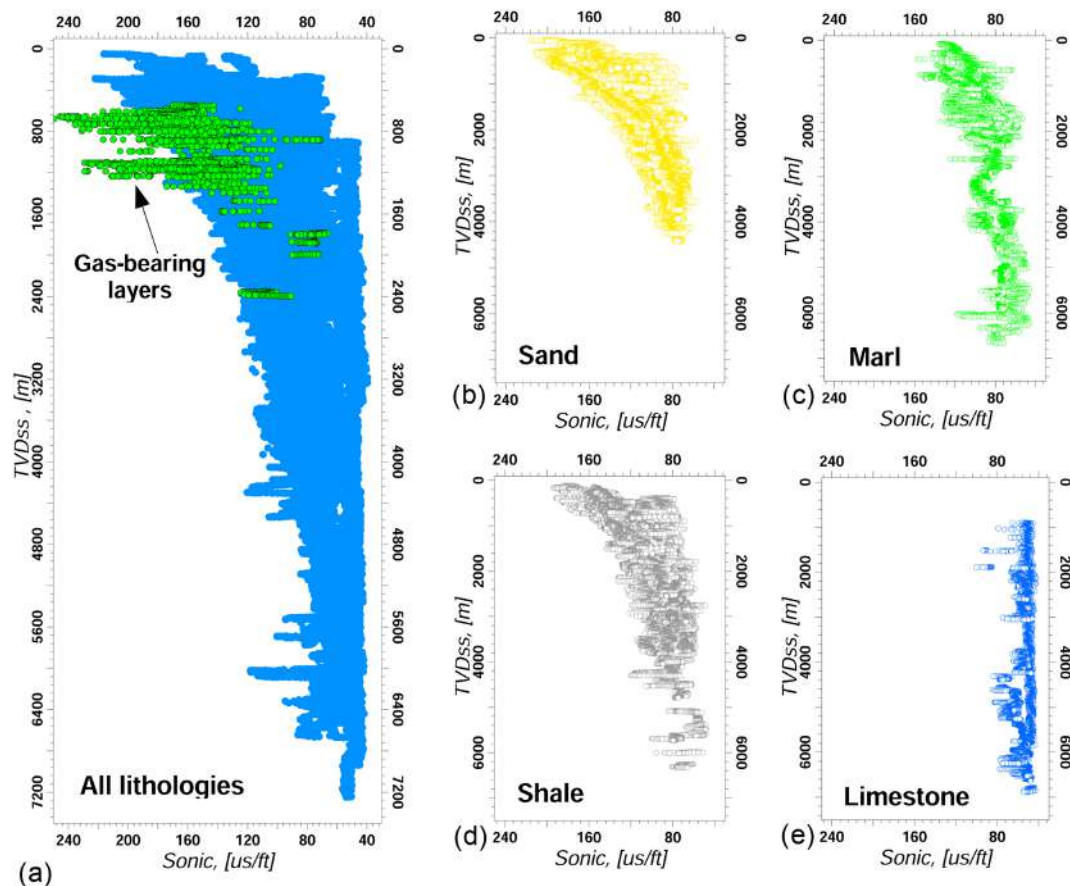


Figure 8. (a) Variation of transit time with depth for all samples showing the effect of the presence of gas. (b–e) Variation of transit time with depth for the sand, marl, shale, and limestone lithologies.

increasing depth (Fig. 8b–d), and at about 4 km depth, the transit time flattens out, showing rather constant values for higher depths, independently from the lithology. The continuous decrease of the P wave transit time with depth reflects the increasing compaction of the sediments due to the overburden weight. The limestone is an exception, showing a relatively constant transit time independently of the depth. The presence of gas significantly increases the transit time with respect to water-saturated rocks: the so-called gas effect is outlined as a rock density reduction (Fig. 8a).

The abundance of each lithology within the main units defined in this study significantly affects the average mechanical rock properties of the entire unit (Fig. S2 in the Supplement). One of the advantages of the analysis performed is the possibility of assigning specific mechanical properties for each lithology and for different depths. Knowing the amount of each lithology present in the geological units, we can achieve a more precise characterization of the subsurface geological layers, which is fundamental for improving the quality of the geomechanical simulations. Applications of the sonic log analysis in defining mechanical rock properties of the subsurface of the Po Plain area can be found in Bene-

tatos et al. (2023a, b). In the first work, the authors propose a workflow for geomechanical simulations through seabed monitoring. A significant step in the workflow involves the rock mechanical characterization that is performed through the analysis of the sonic log data that are converted to dynamic Young's modulus values that are specific to the different lithologies and to various depths. The same approach is also followed by Benetatos et al. (2023b) to calculate the mechanical properties of the Argille del Santerno Fm. They used well log data and compared them to those derived from laboratory analysis of core samples. This comparative analysis revealed relations between well log and laboratory-derived properties and contributed to the understanding of the deformation behaviour of this important geological formation that extends across northern Italy.

4.2 Geological cross-sections

We collected 6341 km of published geological cross-sections (Cassano et al., 1986; Lindquist, 1999; Casero, 2004; Picotti et al., 2007; Fantoni and Franciosi, 2009; Toscani et al., 2009; Wilson et al., 2009; Boccaletti et al., 2011; Pola et al., 2014; ISPRA, 2015; Maesano et al., 2015; Turrini et al., 2015; Li-

vani et al., 2018; Table 1). Several procedures were implemented for uploading, calibrating, and revising the geological cross-sections in a 3D environment and, finally, for digitizing the selected horizons. The location maps (i.e. maps displaying the section traces) and the cross-sections were graphically re-arranged and improved to reduce imperfections and errors due to the low quality and/or image distortion. We then georeferenced the location maps in the QGIS environment, digitizing the relative section traces (Fig. 4). Based on the geographically oriented section traces, the cross-section images (raster format) were properly uploaded in a 3D environment. The geological cross-sections composed of segments with different orientations were cut into several parts and separately imported. Where necessary (i.e. location inconsistency), the geological cross-sections were repositioned using the intersections with other data such as wells, surface geology (e.g. geological boundaries, faults), other geological cross-sections, and orographic and hydrographic features (e.g. rivers).

The revised and georeferenced cross-sections were finally uploaded into a 3D project in the Petrel® software. We digitized four geological horizons that roughly correspond to the boundaries of the main lithological discontinuities recognized through the well data analysis. The horizons are, from the oldest to the youngest, as follows: the top of the carbonate succession (more marly in its upper portion), which divides a mainly carbonate succession (below) by a mainly siliciclastic succession (above), and it does not represent a chronostratigraphic boundary; the Pliocene base; the Calabrian base; and the base of recent continental deposits. In the regions characterized by a vertical duplication of the same unit due to the effect of thrusting, we digitized the hanging wall of the units until the hanging wall cut-off and then passed on directly to the footwall of the same unit. In such a way, a marked artificial step was generated; however, we deem this approximation to be necessary for the successive 3D modelling dataset creation, which does not integrate any fault element. In the data collection process, some public geological cross-sections were excluded from the database and the digitization process. For instance, the AGIP geological cross-sections reported in the Italian geological maps at 1 : 100 000 scale (sheets 75, 77, and 88; <https://www.isprambiente.gov.it/it/attivita/suolo-e-territorio/cartografia/carte-geologiche-e-geotematiche/carta-geologica-alla-scala-1-a-100000>, last access: 11 May 2021) were not used due to the geological interpretation based on scarce deep-data information (many deep wells and seismic reflection profiles were unavailable at that time), strongly differing from interpretations recently proposed on the basis of a large amount of subsoil data. Furthermore, some vintage sections (i.e. Bally et al., 1986) were excluded since some more recent geological cross-sections passing close to their traces show a more precise localization and better graphical properties, allowing for a more accurate digitization process.

For each digitized horizon, a delimited text file in ASCII format reporting the *xyz* coordinates is generated. Since the digitization process was performed manually, the data are provided with an irregular sampling step.

4.3 Geological maps

The 3D database also includes data derived from 10 published subsurface geological maps. We digitized the following maps:

- two isobath maps of the base of the recent continental deposits (QC1 horizon map by ISPRA, 2015; Scardia et al., 2012)
- one isobath map of the Calabrian base (QM1 horizon map by ISPRA, 2015)
- two isobath maps of the Pliocene base (Bigi et al., 1990a, b; ISPRA, 2015)
- four isobath maps of the carbonate succession top (Casero et al., 1990; Nicolich et al., 2004; ISPRA, 2015; D’Ambrogi et al., 2023)
- one isobath map of the magnetic basement top (Cassano et al., 1986).

The maps, available in hard copy and/or in raster format, were graphically revised and re-arranged in order to reduce possible scanning defects and distortions. The maps were then georeferenced, and the contour lines were digitized using QGIS software. The digitized contour lines were exported and uploaded into the 3D Petrel® database. We then verified in a 3D environment their consistency with other subsurface geological information, especially well data.

For each map, a delimited text file in ASCII format reporting the *xyz* coordinates of the contour lines was generated. Since the digitization process was performed manually, the data are provided with an irregular sampling step.

5 Data accuracy

A widespread accepted standard approach to address map accuracy is still not available. Recent studies suggest methods and standards for error analysis of geological or subsurface maps (e.g. Kint et al., 2020, and references therein). However, these methods are still affected by significant bias as they depend on the data availability and the criteria of data selection. Quality flagging is the basic approach used to quantify uncertainty within a spatial dataset and is done by assessing metadata fields. This method can be limited to indicate the presence or absence of data, or it can be very complex, producing a full range of quantitative error ranges (e.g. Bardossy and Fodor, 2001). Kint et al. (2020) presented an approach to assess data uncertainty for a well dataset in the Quaternary succession of the Belgian Continental Shelf.

They produced confidence maps based on datasets from different origins and time periods. Their method consists of the following: (i) determination of the data density (how much data contribute to each grid cell to provide information on lateral and depth variability), (ii) direct mapping of measured errors and accuracies, (iii) transformation of the measured values or categorical quality flags into uncertainty percentages, and (iv) selection of data subsets based on the uncertainty maps. Not all these points are always feasible or necessary. This renders the method non-general. For example, in the case of few data or datasets without associated uncertainty, steps (ii) and (iv) are not recommended or feasible. Furthermore, the uncertainty drags errors due to the fact that instrumental (absolute accuracy, positioning accuracy) and human (expert judgement, data selection, data origin and representation) accuracy are often not quantifiable.

The only universal and dataset-unrelated rule when considering the geographic space comes from the first law of geography (Tobler, 1970) that states “everything is related to everything else, but near things are more related than distant things”. This law is the foundation of the concepts of spatial dependence and spatial auto-correlation and is used specifically for the inverse distance weighting method for spatial interpolation (Shepard, 1968).

Generalizing the approach proposed by Kint et al. (2020) with an application to arbitrary spatial data and using the inverse distance weight (IDW) for our analysis, we implemented, in a preliminary way, a method to weight the accuracy and/or confidence of geological surfaces. For each horizon, we quantified the following: (i) the data density contributing to the assessment of the lateral accuracy and the depth variability; (ii) the accuracy based on the data density and the spatial autocorrelation converted into a probability (inverse distance weight – IDW), describing the confidence of the data at each point of the study area; and (iii) the error associated with the depth of the geological surfaces due to discrepancies between the data of different origins where different guesses exist. Hence, for each point of the study area, we provided a value indicating the accuracy and a value indicating the estimated error of the depth of the geological surface.

To apply our model, we started by edging the study area including the observation region and covering it through an evaluation grid (Fig. 9a). In surface and subsurface mapping, the observations come from properly identified sites. The locations of these sites (hereafter checkpoints) are known and tag the observations. The variable of interest (i.e. horizon depth) exists in every point of the region (i.e. grid nodes) but is observed only in a finite set of locations (checkpoints). The variability model describes how uncertainties increase moving away from the checkpoint with respect to the best guess, built according to the observations and the geological constraints. In our case study, the properly identified sites are points (wells), lines (the traces of geological cross-sections digitized at discrete points), and polygons (here intended as

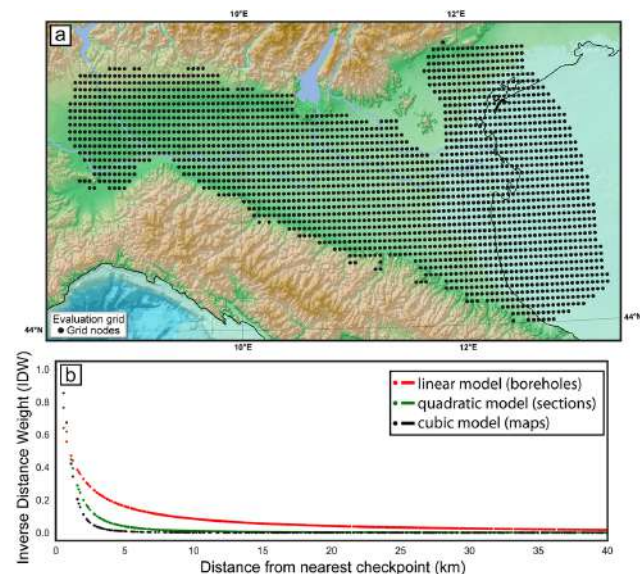


Figure 9. (a) Grid nodes used to evaluate the data accuracy and uncertainties for geological surfaces presented for the study area. At each node, based on spatial autocorrelation, we calculated the inverse distance weight (IDW) with respect to point observations (checkpoints). (b) The model adopted for the IDW describes how uncertainties increase, moving away from the best guess at checkpoints (i.e. at wells, along geologic cross-sections, or on depth maps); at the same distance from a checkpoint, well data give higher IDWs (red points) in comparison to data derived from geological cross-sections or interpolated maps (green and black points).

raster fields digitized at discrete points, i.e. isobaths of geological maps). Note that not all kinds of checkpoints can be considered at the same level of confidence since well data give better depth constraints to those derived from geological cross-sections or interpolated maps. For this reason, it is convenient to assign higher specific weights to first-order checkpoints (well data in our case) with respect to higher-order checkpoints (sections or maps). Once the hierarchical subdivision has been made, the inverse distance (ID) principle is used to model the uncertainties at each point of the study area (i.e. at grid nodes) based on spatial autocorrelation with respect to checkpoints:

$$ID = \frac{1}{1 + r^p}, \quad (1)$$

where ID is the inverse distance, r is the distance between the point of observation and the checkpoint, and p is the checkpoint order; in this study, $p = 1$ for well data, $p = 2$ for sections, and $p = 3$ for maps. The inverse distance (ID) is then normalized to obtain the inverse distance weight IDW as follows:

$$IDW = \frac{ID - ID_{\min}}{ID_{\max} - ID_{\min}}. \quad (2)$$

The IDW assigns a confidence based on distance autocorrelation that decreases more gently when considering first-order

Table 5. Parameters of each unit. Checkpoint refers to the number of locations where the data are observed. P is the checkpoint order, where $p = 1$ for well data, $p = 2$ for sections, and $p = 3$ for maps.

Lithological surface	Grid points	No. of checkpoints ($p1$)	No. of checkpoints ($p2$)	No. of checkpoints ($p3$)	No. of checkpoints (total – point density)
Base of recent continental deposits	2334	42	634	3082	3758 – 1.61
Calabrian base	2334	139	3065	2299	5503 – 2.36
Pliocene base	2334	114	4238	29 795	34 174 – 14.63
Carbonate top	2334	17	3309	169 785	173 111 – 74.17

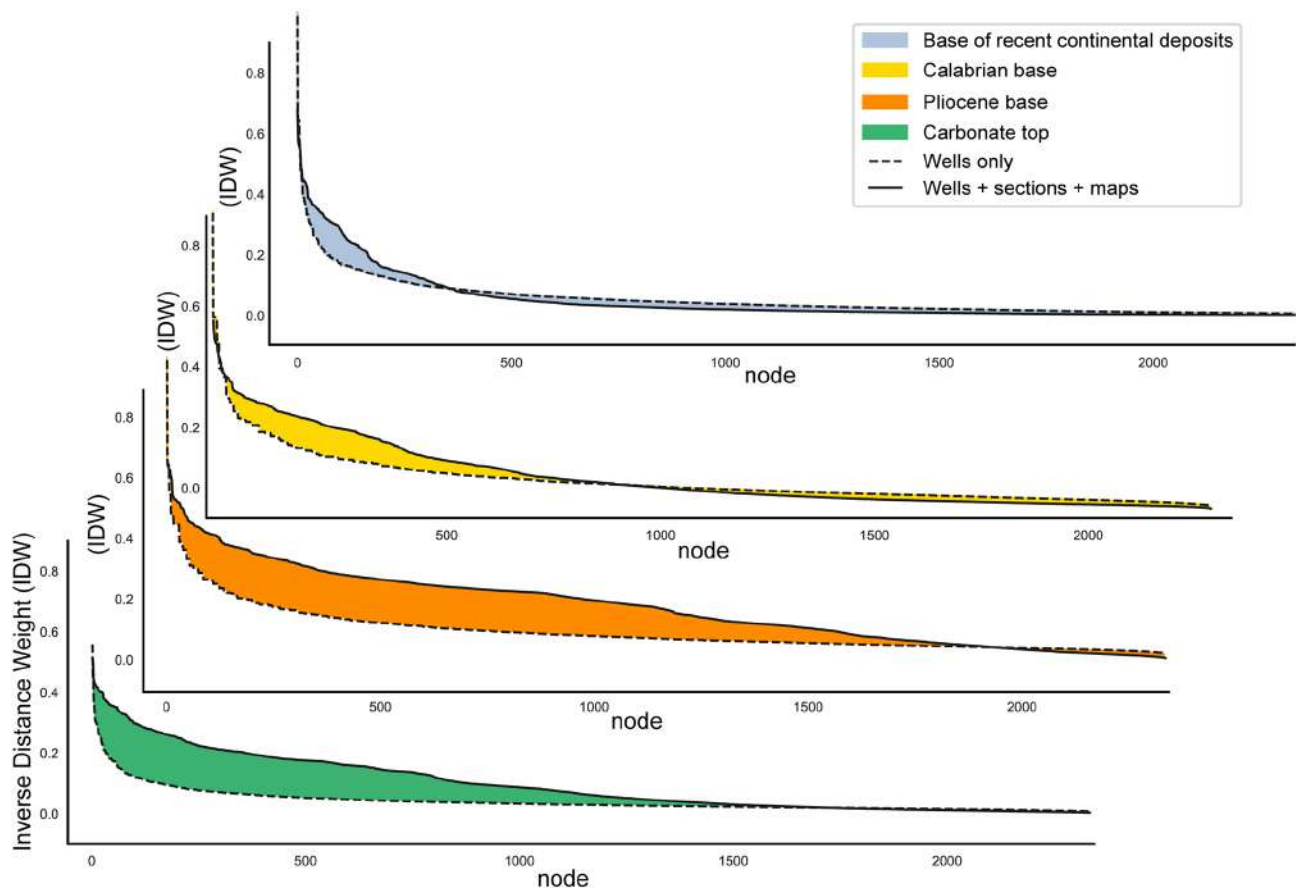


Figure 10. IDW values at grid nodes calculated for each surface considering distances from well data only (dashed lines) or integrating distances from well data plus geological cross-section plus geological maps (solid lines). The area between the two lines for each proposed surface is larger for greater uncertainties. Note that the uncertainties increase with the depth of the surfaces and that the total number of checkpoints does not always increase the confidence level of the data (as, for example, in the recent continental deposits).

checkpoints (red curve goes under 0.2 at a distance of 7 km; Fig. 9b) with respect to higher-order checkpoints (green and black curves go under 0.2 at a distance of 2 km; Fig. 9b). The total weight calculated at each point of the study area is the mean value of the weights calculated with respect to different-order checkpoints. This means that $IDW = 1$ is the best guess assigned to grid nodes that, in the ideal case, lie – at the same time – over checkpoints of order 1 to n (i.e. in our case, over a well crossed by a section and coinciding with an

interpolation point of the map). Statistics of the dataset are reported in Table 5.

5.1 Data density

Four out of the five processed geological surfaces (i.e. the base of recent continental deposits, the Calabrian base, the Pliocene base, and the carbonate succession top) were reconstructed using checkpoints of order 1 (i.e. well data), 2 (i.e. geological cross-sections), and 3 (i.e. subsurface geological

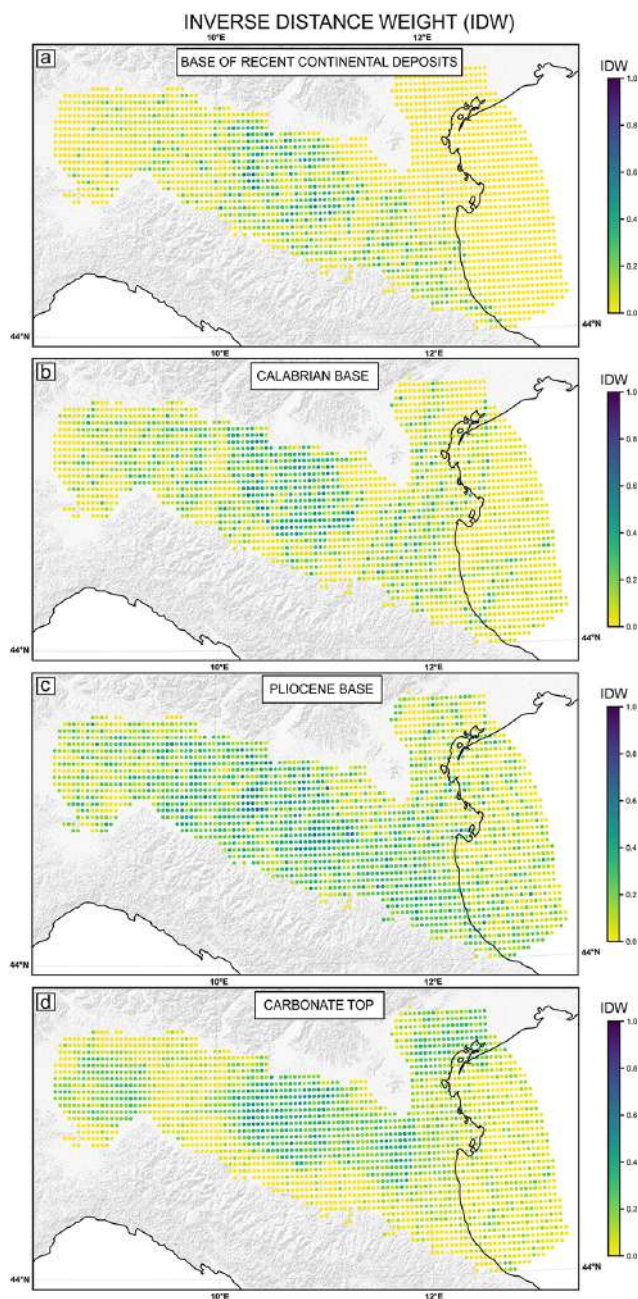


Figure 11. The spatial distribution of the IDW for the four analysed surfaces. The IDW values represent the confidence of the variable of interest (level depth) at each node of the grid (1 indicates max confidence).

maps). The reconstruction of the magnetic basement top derives from a unique source (Cassano et al., 1986), and, for this reason, we avoided including this surface in the data accuracy analysis.

The analysis of our dataset (Table 5) shows that the three shallowest surfaces (i.e. recent continental deposits, Pleistocene base, and Pliocene base) are the most constrained with up to 139 checkpoints of the first order, whereas the carbon-

ate succession top is constrained by a few checkpoints of order 1. The carbonate succession top and the Pliocene base are described by the highest amount of data, with a density larger than 74 total checkpoints to each grid cell.

5.2 Data analysis

The total number of checkpoints does not always increase the confidence level of the data. In fact, for the Calabrian base, the Pliocene base, and the carbonate succession top, the IDW values also increase by up to double the amount when calculated considering checkpoints of all orders, whereas they decrease for recent continental deposits (dashed lines in Fig. 10). In the latter case, higher confidence is obtained when considering only the order-1 checkpoints (solid lines in Fig. 10). The best-constrained surface is confirmed to be the Pliocene base, with a high number of both well data (i.e. order-1 checkpoints) and total data. The spatial distribution of the IDW for the proposed surfaces is reported in Fig. 11 and represents the confidence in the variable of interest (level depth) at each node of the grid (1 indicates maximum confidence). All the maps show maximum IDW ≈ 0.7 and a mean value of 0.06 (recent continental deposits – Fig. 11a), 0.09 (Calabrian base – Fig. 11b), 0.14 (Pliocene base – Fig. 11c), and 0.08 (carbonate top – Fig. 11d). The IDW values indicate that the Pliocene surface has a confidence level almost double than that obtained for the other surfaces on average. Interactive figures (HTML format to be opened in a web browser) of each map reported in Fig. 11 are available in the Supplement (S1.zip) and provide detailed statistical information at each node of the interpolation grid.

5.3 Uncertainty associated with depth

The four surfaces analysed in this work derive from different origins and types of data (see Sect. 3; only the magnetic basement top derives from a unique source). The variability in quality, periods of creation, owners, and compiler sensibility (human error) of the datasets produces large – not quantifiable – uncertainty affecting the input data. Furthermore, since most of the collected public data derive from interpretations of seismic profiles, the data in depth are strongly influenced by the velocity model used for the depth conversion. Unfortunately, most of the primary data are not provided along with the used velocity model, and for this reason, it was not possible to take into account this variable. Further, the study area is non-uniformly described by the dataset.

Each grid node is associated with one to four values of depth depending on the number of available identified sites (i.e. checkpoints from different sources) coinciding with that node. Hence, it turns out that it is possible to calculate the maximum and minimum depth of each surface at each node if at least two depth values are available in that specific node. The range of depths at the nodes represents the uncertainty of the level description. Figure 12 shows the depth variation

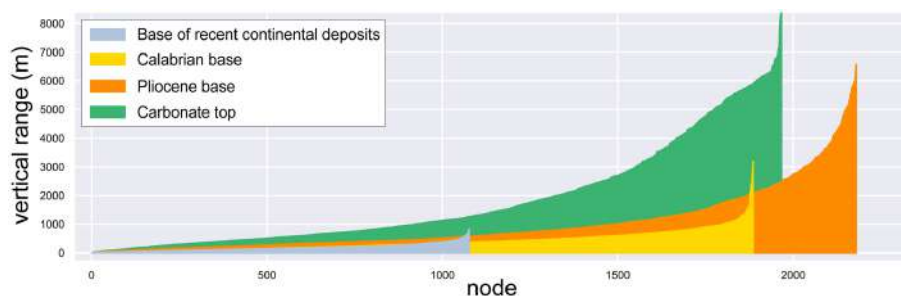


Figure 12. Range of depth variations interpolated at each point of the evaluation grid based on the different datasets available for the four surfaces.

for the four surfaces calculated considering the maximum and minimum values for each node with at least two values. The bottoms of recent continental deposits (light-blue band) and of the Pleistocene unit (yellow band) show a small variation in depth (< 3 km) in comparison to the Pliocene (orange band – up to 6 km) and carbonate (green band – up to 8 km) bases. The maps in Fig. 13 illustrate the geographic distribution of depth evaluation uncertainty. Interactive figures of each map reported in Fig. 13 are available in the Supplement (S1.zip).

6 Derived data: methods and results

The construction of an accurate 3D geological model requires good coverage and consistency of the source data. Improving the multi-source data consistency helps to avoid errors and distortions during the 3D model generation. To ensure the most significant data coverage and consistency in the area, we revised, compared, and finally integrated the collected primitive data (i.e. wells, geological cross-sections, and maps).

Based on the data accuracy analysis and the uncertainty associated with level depth (see Sect. 5), we totally or partially removed the digitized primitive data showing the highest discrepancy with other data. For this purpose, as mentioned in the previous section, we assigned a priority order to the data according to their type. The highest priority is attributed to well data as they give the best depth constraint of the units (order-1 checkpoints). Hence, the well data represent the main control points of our model, and none of them were excluded during the integration process. Regarding geological cross-sections and maps, if a difference in the depth of the surface is observed (Fig. 13), we kept those data showing the best fit with the well data. In other cases, we kept the most recent data, except when they were very discordant from the average data (for example, geological sections with a horizon depth very different from that indicated by other more reliable data) or from the predominant interpretative schemes (for example, geological cross-sections with a tectonic style completely different from the preponderant interpretations). In particular, it should be pointed out that the

base of recent continental deposits is defined from well data and the isobath map reported in Scardia et al. (2012), which integrates the aquifer data of the Lombardy (Regione Lombardia and Eni-AGIP, 2002) and Emilia Romagna regions (Regione Emilia Romagna and Eni-AGIP, 1998). The inconsistent data removal was performed manually. These revised data integrated with the top of the magnetic basement, the only unit deriving from a single source (i.e. Cassano et al., 1986) and hence without any integration, were collected in ASCII format, reporting the xyz coordinates of the digitized data.

We eventually constructed a 3D geological model of the rock volume interposed between the magnetic basement top and the topographic surface (middle Triassic–present) by means of the revised primitive data. To define the top of the modelled rock volume, since our study area is located both offshore and onshore (Fig. 2), we joined the land topography, deriving from a public digital elevation model of the whole Italian territory at an original resolution of 10 m cell size (Tarquini et al., 2007), with the bathymetry of the offshore area (<https://www.gebco.net/>, last access: 15 March 2018). The 3D geological model is made up of unfaulted surfaces obtained by gridding the revised and integrated multi-source primitive data. For the gridding process, we applied in Petrel® software a convergent interpolation algorithm with a 250 m sampling step. After gridding, we quality-checked and, where necessary, manually improved the modelled surfaces. The 3D model does not integrate any fault element. Thus, the modelled surfaces do not show any dislocation but rather shows sudden height differences in correspondence with the major tectonic structures, mostly where thrust sheets produce the vertical superimposition of the same unit (Fig. 14). The accuracy of the derived geological surfaces mainly depends on the quality and the quantity of source data (i.e. primitive data).

The aforementioned gridded surfaces represent the main boundaries that define units with different mechanical behaviour and subdivide the model into the following five sub-volumes, from top to bottom: the continental portion of the Quaternary deposits, the Pleistocene Asti sands, the Pliocene sands (i.e. Santerno, Porto Corsini, and Porto Garibaldi sand-

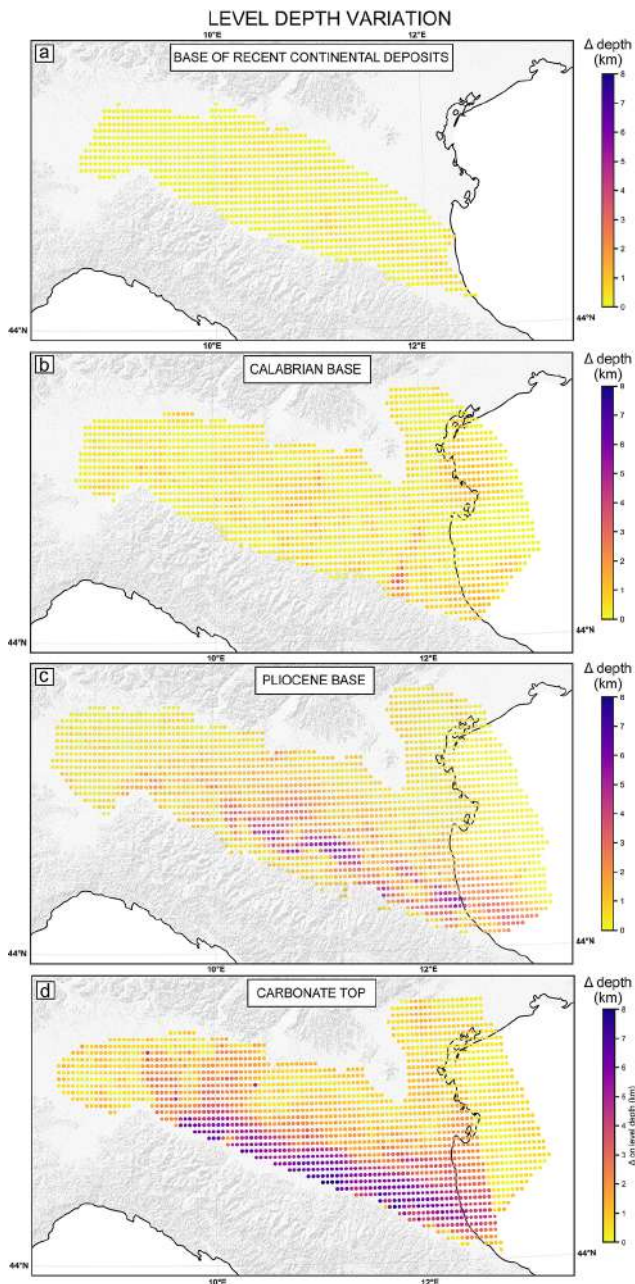


Figure 13. Geographic distribution of the range of depth variations for the four analysed surfaces. It is useful to compare these data with the IDW values in Fig. 11 in order to obtain more complete and comprehensive information.

stones), the upper Eocene to Messinian siliciclastic formations (i.e. Gonfolite-Gallare Marls, Marnoso Arenacea Fm., San Donà Marls, Glausconie di Cavanella Fm., Fusignano Fm., Sergnano gravels, etc.), and the carbonate-marly succession.

The base of the recent continental deposits (Fig. 14a) was reconstructed in a restricted area, where it was intercepted by wells and modelled in the literature (Scardia et al., 2012).

Areas with recent prodelta, delta, and marine sediments have been excluded (Fig. 14a). The base of the recent continental deposits consists of a slightly articulated surface that generally deepens from the peripheral sectors of the model area to the median areas of the Po valley. It is characterized by a depocenter area located between the Emilia and Ferrara arcs, where it reaches its maximum depth in the Parma area. The accuracy of this surface is generally intermediate, with a strong constraint given by the isobath map digitized from Scardia et al. (2012) (Fig. 4).

The Calabrian base (Fig. 14b) generally delimits the lower contact between the Asti sands and the Gelasian and Pliocene sandstones, except where, due to the erosion affecting the anticline culminations (in correspondence with the Emilia and Ferrara arcs), the Pleistocene deposits are unconformably in contact with the Miocene ones (on the top of the Emilia Arc anticlines). This surface progressively deepens from the model borders to the inner part of the Po Plain, except in the Ferrara Arc area, where some culminations can be observed. It reaches its maximum depth in the Parma–Mantova area and in the coastal and northern Adriatic areas. The accuracy of this surface is variable but generally well constrained by most of the available geological cross-sections and numerous wells. Moreover, in the Brescia–Mantova area, it is constrained by an accurate depth contour map (ISPRA, 2015; Fig. 4c).

The Pliocene base covers almost the entire area except for the Emilia and Ferrara anticlines, where it was eroded due to the tectonic uplift (Fig. 14c). This lithological boundary shows a rather articulated morphology characterized by pronounced culmination (located on the main anticline axes of the Emilia and the Ferrara arcs) and depocenter areas (between the Emilia and Ferrara arcs, immediately south of the Ferrara Arc, and in the coastal area). The accuracy of this surface is variable, but it is generally constrained by a large number of wells, geological cross-sections, and two subsurface geological maps covering the entire model area (Bigi et al., 1990a, b) and the GEOMOL project study area (ISPRA, 2015; Fig. 4c).

The carbonate succession top separates the siliciclastic formations (upper Eocene–present) from the carbonate and marly ones (Triassic to middle–upper Eocene in age). This surface deepens from NE to SW (beneath the northern Apennine front), with a local and pronounced elevation at the Ferrara Arc, where carbonates were markedly uplifted by the Apennine orogenic process (Fig. 14d). The accuracy of this surface is variable. It is constrained by several geological cross-sections but, due to its considerable depth, only a few deep well data items, mostly located on the anticline culminations. Three geological maps located in the eastern portion of the model (Casero et al., 1990; Nicolich et al., 2004) and in the central portion of the model (D’Ambrogi et al., 2023) constrain the surface of the carbonate succession top (Fig. 4c).

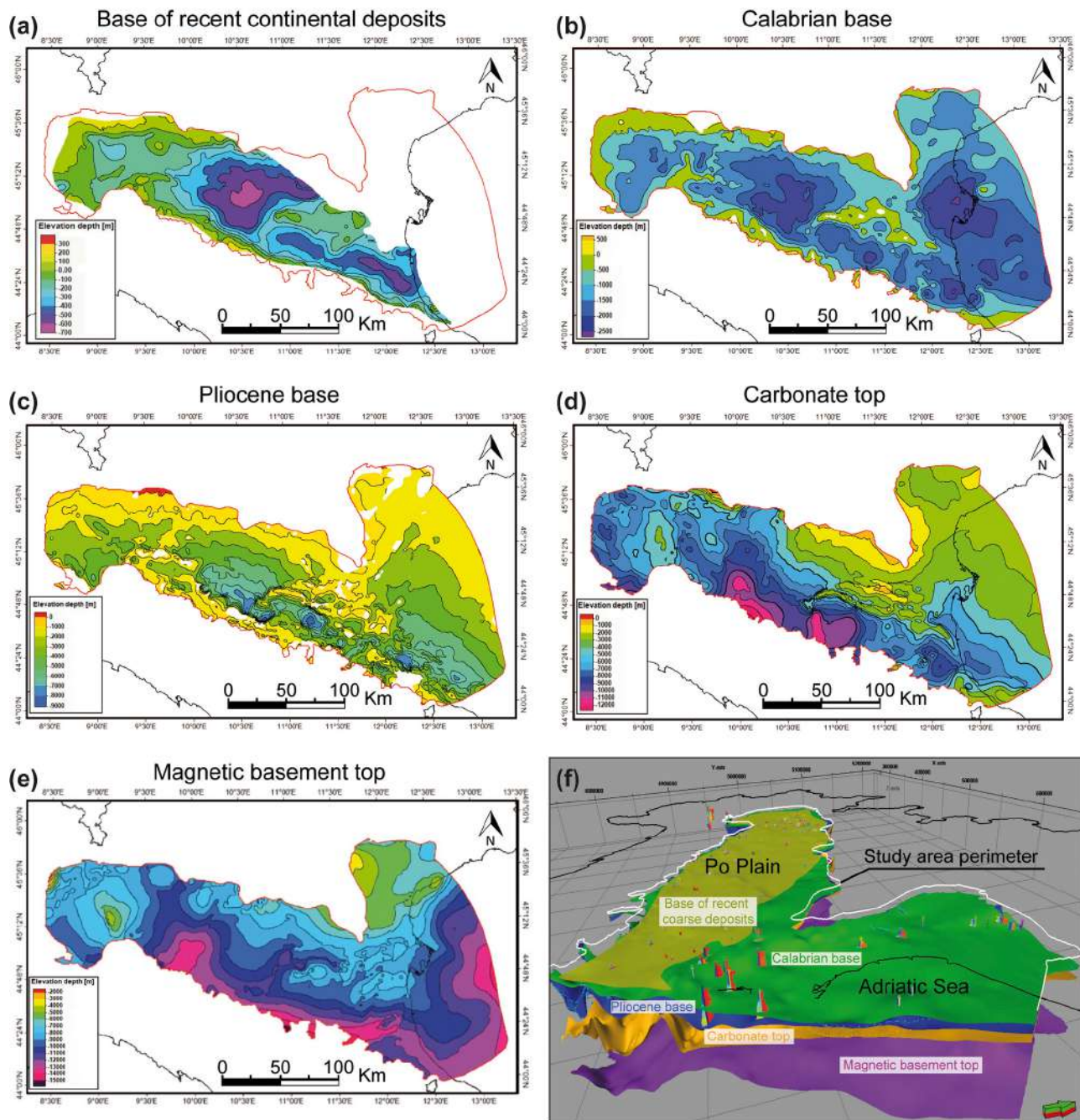


Figure 14. (a–e) Geological maps representing the gridded surfaces generated with the revised primitive data: (a) base of the recent continental deposits, (b) Calabrian base, (c) Pliocene base, (d) carbonate succession top, (e) magnetic basement top. (f) Example of the data digitized and the geological model in 3D view cut along a SW–NE-oriented section.

As mentioned above, the gridded magnetic basement top (Fig. 14e) is based on the published depth contour map by Cassano et al. (1986); consequently, its accurateness depends only on the source data accuracy.

7 Data availability

Primitive and derived data are available for open access in ASCII format at the following link: <https://doi.org/10.5281/zenodo.8126519> (Livani et al., 2023). The format and the organization of data are explained in the related description file.

The dataset can be imported into any software handling 3D geological data, well data information, and spatial vector data formats.

8 Conclusions

The database provides a collection of geological and geophysical data of the Po Plain subsurface and of the northern Adriatic Sea; these were collected and digitized from the literature and from open repositories. We digitized data from the composite logs of 160 wells drilled in the area. Borehole information (i.e. wellhead coordinates, rotary table elevation, measured depth, true depth, total depth, and deviation survey) and spontaneous potential, gamma ray, and sonic logs are provided in ASCII format. Five horizons were digitized from 61 geological cross-sections and from 10 geological maps, ordered as follows from the oldest to the youngest: the top of the magnetic basement, the top of the carbonate succession, the base of the Pliocene, the base of the early Pleistocene (i.e. near top Gelasian; see Sect. 3), and the base of recent continental deposits. The digitized data are provided in ASCII format, reporting the *xyz* coordinates of the digitized surfaces.

Through an accuracy analysis performed on the primitive data and their subsequent processing, a new set of data has been created (i.e. derived data). Since the primary data show a depth uncertainty, we accurately revised the primary data by integrating only the data showing the best fitting. From these data, we generated a simplified 3D geological model characterized by several gridded surfaces of the main geological units (Fig. 14f).

Through the elaboration of the digitized logs, it is possible to directly extract geophysical and mechanical properties of the rock volume interposed between the gridded surfaces (e.g. P wave velocity) and to obtain further derived properties. For example, sonic velocities can be converted to mechanical rock properties, such as Young's modulus or Poisson ratio, that find applicability in geomechanical simulations which are performed to evaluate the ground subsidence and/or uplift phenomena (Carminati and Di Donato, 1999; Benetatos et al., 2017; Antoncicchi et al., 2021) or the change of stress field in a specific area in response to natural processes or anthropic activities (e.g. Schutjens et al., 2010; Radwan and Sen, 2021; Hemami et al., 2021; Sangnimnuan et al., 2021).

The dataset developed in the present work supports applications in a wide range of research areas with benefits for scientists, practitioners, and decision makers. As an example, once populated with the values of seismic velocity, the 3D geological model can find several applications in seismological studies. It can be used to improve the procedure and to reduce the uncertainties during earthquake location, it can contribute to the calculation of more accurate focal mechanisms, and it can perform wave propagation and ground motion sim-

ulations (e.g. Magistrale et al., 1999; Süss et al., 2001; Molinari et al., 2015; Livani et al., 2022). The 3D model also represents a starting model in perturbation studies, such as linearized inversions of travel times for crustal velocities (e.g. Magistrale and Day, 1999) or for studies related to the seismic waveforms for crustal structure; moreover, it can be used to derive densities and to compare them to gravity observations (Roy and Clayton, 1999).

In conclusion, this database will be useful in better defining and mitigating the possible natural and anthropogenic risks for the preservation of the environment and the safeguarding of the social and economic interests of the territory, contributing to a better and more efficient management of subsoil resources.

Supplement. The supplement related to this article is available online at: <https://doi.org/10.5194/essd-15-4261-2023-supplement>.

Author contributions. ML: data curation, formal analysis, investigation, methodology, validation, visualization, writing – original draft preparation. LP: conceptualization, data curation, methodology, project administration, supervision, validation, visualization, writing – original draft preparation. CB: conceptualization, data curation, formal analysis, investigation, methodology, supervision, validation, visualization, writing – original draft preparation. FM: data curation, formal analysis, methodology, investigation, writing – review and editing. AB: conceptualization, project administration, supervision, methodology, writing – review and editing. EC: conceptualization, project administration, supervision, writing – review and editing. CD: project administration, supervision, writing – review and editing. PP: data curation, formal analysis, validation, visualization, writing – original draft preparation. RM: data curation, formal analysis, investigation, validation, writing – review and editing. GC: data curation, formal analysis, investigation, writing – review and editing. VR: conceptualization, supervision, writing – review and editing. FV: conceptualization, project administration, supervision, writing – review and editing. IA: supervision, writing – review and editing.

Competing interests. The contact author has declared that none of the authors has any competing interests.

Disclaimer. Publisher's note: Copernicus Publications remains neutral with regard to jurisdictional claims in published maps and institutional affiliations.

Acknowledgements. This research is performed within the “CLYPEA – Innovation Network for Future Energy”, “subsoil deformations” project, promoted by the Ministero dell'Ambiente e della Sicurezza Energetica. The authors are grateful to Chiara D'Ambrogi and Roberto De Franco for their valuable suggestions

and discussions. Finally, we kindly thank two anonymous reviewers for their constructive and useful comments.

Financial support. This research has been supported by the Ministero dell’Ambiente e della Sicurezza Energetica (formerly Italian Economic Development Ministry).

Review statement. This paper was edited by Giulio G. R. Iovine and reviewed by two anonymous referees.

References

- Amadori, C., Toscani, G., Di Giulio, A., Maesano, F. E., D’Ambrogio, C., Ghielmi, M., and Fantoni, R.: From cylindrical to non-cylindrical foreland basin: Pliocene–Pleistocene evolution of the Po Plain–Northern Adriatic basin (Italy), *Basin Res.*, 31, 991–1015, <https://doi.org/10.1111/bre.12369>, 2019.
- Amorosi, A. and Milli, S.: Late quaternary depositional architecture of Po and Tevere River deltas (Italy) and worldwide comparison with coeval deltaic successions, *Sediment. Geol.*, 144, 357–375, [https://doi.org/10.1016/S0037-0738\(01\)00129-4](https://doi.org/10.1016/S0037-0738(01)00129-4), 2001.
- Antonucci, I., Ciccone, F., Rossi, G., Agate, G., Colucci, F., Moia, F., Manzo, M., Lanari, R., Bonano, M., De Luca, C., Calabrese, L., Perini, L., Severi, P., Pezzo, G., Macini, P., Benetatos, C., Rocca, V., Carminati, E., Billi, A., and Petracchini, L.: Soil deformation analysis through fluid-dynamic modelling and DInSAR measurements: a focus on groundwater withdrawal in the Ravenna area (Italy), *BGTA-Bollettino di Geofisica Teorica ed Applicata*, 62, 301–318, <https://doi.org/10.4430/bgta0350>, 2021.
- Baldi, P., Casula, G., Cenni, N., Loddo, F., and Pesci, A.: GPS-based monitoring of land subsidence in the Po Plain (Northern Italy), *Earth Planet. Sc. Lett.*, 288, 204–212, <https://doi.org/10.1016/j.epsl.2009.09.023>, 2009.
- Bally, A. W., Burbi, L., Cooper, C., and Ghelardoni, R.: Balanced sections and seismic reflection profiles across the Central Apennines, *Mem. Soc. Geol. It.*, 35, 257–310, 1986.
- Bardossy, G. and Fodor, J.: Traditional and new ways to handle uncertainty in geology, *Nat. Resour. Res.*, 10, 179–187, 2001.
- Benetatos, C., Codegone, G., Deangeli, C., Giani, G., Gotta, A., Marzano, F., Rocca, V., and Verga, F.: Guidelines for the study of subsidence triggered by hydrocarbon production, *Geingegneria Ambientale e Mineraria*, 152, 85–96, 2017.
- Benetatos, C., Codegone, G., Ferraro, C., Mantegazzi, A., Rocca, V., Tango, G., and Trillo, F.: Multidisciplinary analysis of ground movements: an Underground Gas Storage case study, *Remote Sens.*, 12, 3487, <https://doi.org/10.3390/rs12213487>, 2020.
- Benetatos, C., Catania, F., Giglio, G., Pirri, C. F., Raeli, A., Scaltrito, L., Serazio, C., and Verga, F.: Workflow for the Validation of Geomechanical Simulations through Seabed Monitoring for Offshore Underground Activities, *J. Mar. Sci. Eng.*, 11, 1387, <https://doi.org/10.3390/jmse11071387>, 2023a.
- Benetatos, C., Rocca, V., Verga, F., Adinolfi, L., and Marzano, F.: Deformation behavior of a regional shale formation from integrated laboratory and well data analysis: Insights for underground fluid storage in northern Italy, *Geoenergy Science and Engineering*, 229, 212109, <https://doi.org/10.1016/j.geoen.2023.212109>, 2023b.
- Bertotti, G., Picotti, V., Bernoulli, D., and Castellarin, A.: From rifting to drifting: Tectonic evolution of the south-Alpine upper crust from the Triassic to the Early Cretaceous, *Sedim. Geol.*, 86, 53–76, [https://doi.org/10.1016/0037-0738\(93\)90133-P](https://doi.org/10.1016/0037-0738(93)90133-P), 1993.
- Bigi, G., Castellarin, A., Coli, M., Dal Piaz, G. V., Sartori, R., Scandone, P., and Vai, G. B.: Structural Model of Italy scale 1 : 500.000, sheet 1, C.N.R., Progetto Finalizzato Geodinamica, SELCA Firenze, 1990a.
- Bigi, G., Castellarin, A., Coli, M., Dal Piaz, G. V., and Vai, G. B.: Structural Model of Italy scale 1 : 500.000, sheet 2, C.N.R., Progetto Finalizzato Geodinamica, SELCA Firenze, 1990b.
- Bitelli, G., Bonsignore, F., Del Conte, S., Franci, F., Lambertini, A., Novati, F., Severi, P., and Vittuari, L.: Updating the subsidence map of Emilia-Romagna region (Italy) by integration of SAR interferometry and GNSS time series: the 2011–2016 period, *Proc. IAHS*, 382, 39–44, <https://doi.org/10.5194/piahs-382-39-2020>, 2020.
- Boccaletti, M., Coli, M., Eva, C., Ferrari, G., Giglia, G., Lazzarotto, A., Merlanti, F., Nicolich, R., Papani, G., and Postpischl, D.: Considerations on the seismotectonics of the northern Apennines, *Tectonophysics*, 117, 7–38, 1985.
- Boccaletti, M., Bonini, M., Corti, G., Gasperini, P., Martelli, L., Piccardi, L., Tanini, C., and Vannucci, G.: Active structures of the emilia-romagna, *GNCTS – Atti del 23° Convegno Nazionale/02.11*, 2004a.
- Boccaletti, M., Bonini, M., Corti, G., Gasperini, P., Martelli, L., Piccardi, L. P., Severi, P., and Vannucci, G.: Carta sismotettonica della regione Emilia-Romagna, Scala 1 : 250.000, Note Illustrative, *Serv. Geol. Sismico e dei Suoli, Reg. Emilia Romagna*, SELCA-Firenze, 2004b.
- Boccaletti, M., Corti, G. and Martelli, L.: Recent and active tectonics of the external zone of the Northern Apennines (Italy), *Int. J. Earth Sci.*, 100, 1331–1348, <https://doi.org/10.1007/s00531-010-0545-y>, 2011.
- Braun, T., Danesi, S., and Morelli, A.: Application of monitoring guidelines to induced seismicity in Italy, *J. Seismol.*, 24, 1015–1028, <https://doi.org/10.1007/s10950-019-09901-7>, 2020.
- Bresciani, I. and Perotti, C. R.: An active deformation structure in the Po Plain (N Italy): The Romanengo anticline, *Tectonics*, 33, 2059–2076, <https://doi.org/10.1002/2013TC003422>, 2014.
- Burrato, P., Ciucci, F., and Valensise, G.: Un approccio geomorfologico per la prima individuazione di strutture potenzialmente sismogenetiche nella Pianura Padana, *Atti 18° Convegno Nazionale di Geofisica – ING, Roma*, 1999.
- Burrato, P., Ciucci, F., and Valensise, G.: An inventory of river anomalies in the Po Plain, Northern Italy: evidence for active blind thrust faulting, *Ann. Geophys.*, 46, 865–882, 2003.
- Carminati, E. and Di Donato, G.: Separating natural and anthropogenic vertical movements in fast subsiding areas: the Po plain (N. Italy) case, *Geophys. Res. Lett.*, 26, 2291–2294, 1999.
- Carminati, E. and Doglioni, C.: Alps vs. Apennines: The paradigm of a tectonically asymmetric Earth, *Earth-Sci. Rev.*, 112, 67–96, 2012.
- Carminati, E. and Martinelli, G.: Subsidence rates in the Po Plain, northern Italy: The relative impact of natural and anthropogenic causation, *Eng. Geol.*, 66, 241–255, 2002.

- Carminati, E., Doglioni, C., and Scrocca, D.: Apennines subduction-related subsidence of Venice (Italy), *Geophys. Res. Lett.*, 30, 1717, <https://doi.org/10.1029/2003GL017001>, 2003.
- Carminati, E., Lustrino, M., and Doglioni, C.: Geodynamic evolution of the central and western Mediterranean: Tectonics vs. igneous petrology constraints, *Tectonophysics*, 579, 173–192, <https://doi.org/10.1016/j.tecto.2012.01.026>, 2012.
- Casero, P.: Structural setting of petroleum exploration plays in Italy, in: *Geology of Italy*, edited by: Crescenti, U., d'Offizi, S., Merlini, S., and Sacchi, L., Special publication of the Italian geological society for the IGC 32nd, Florence, 189–199, 2004.
- Casero, P., Rigamonti, A., and Iocca, M.: Paleogeographic relationships during Cretaceous between the Northern Adriatic area and the eastern Southern Alps, *Mem. Soc. Geol. Ital.*, 45, 807–814, 1990.
- Cassano, E., Anelli, A., Fichera, R., and Cappelli, V.: Pianura Padana: interpretazione integrata di dati geologici e geofisici, *Atti del 73° Congresso della Società Geologica Italiana*, Roma, 1986.
- Castellarin, A. and Vai, G. B.: Southalpine versus Po plain apenninic arcs, in: *The origin of Arcs. Development in Geotectonics*, edited by: Wezel, C., 21, Elsevier, Amsterdam, 253–280, 1986.
- Castellarin, A., Eva, C., Ciglia, G., and Vai, G. B.: Analisi strutturale del Fronte Appenninico Padano, *Giornale di Geologia*, 47, 47–75, 1985.
- Cati, A., Sartorio, D., and Venturini, S.: Carbonate platforms in the subsurface of the northern Adriatic Sea, *Mem. Soc. Geol. It.*, 40, 295–308, 1987.
- Codegone, G., Rocca, V., Verga, F., and Coti, C.: Subsidence Modeling Validation Through Back Analysis for an Italian Gas Storage Field, *Geotech. Geol. Eng.*, 34, 1749–1763, <https://doi.org/10.1007/s10706-016-9986-9>, 2016.
- Coward, M. P. and Dietrich, D.: Alpine tectonics; an overview, in: *Alpine Tectonics*, edited by: Coward, M. P., Dietrich, D., and Park, R. G., Geological Society Special Publications, 45, 1–29, 1989.
- Cuffaro, M., Riguzzi, F., Scrocca, D., Antonioli, F., Carminati, E., Livani, M., and Doglioni, C.: On the geodynamics of the northern Adriatic plate, *Rend. Fis. Acc. Lincei*, 21, S253–S279, <https://doi.org/10.1007/s12210-010-0098-9>, 2010.
- Dacome, M. C., Miandro, R., Vettorel, M., and Roncari, G.: Subsidence monitoring network: An Italian example aimed at a sustainable hydrocarbon E&P activity. In *Proceedings of the International Association of Hydrological Sciences (IAHS)*, Nagoya, Japan, 15–19 November 2015, Copernicus GmbH, Göttingen, Germany, 372, 379–384, 2015.
- D'Ambrogio, C., Maesano, F. E., Marino, M., Congi, M. P., and Morone, S.: Geological 3D model of the Po Basin, INFN OAR [data set], <https://doi.org/10.15161/oar.it/76873>, 2023.
- Dercourt, J., Zonenshain, L. P., Ricou, L.-E., Kazmin, V. G., Le Pichon, X., Knipper, A. L., Grandjacquet, C., Sbotshikov, I. M., Geyssant, J., Lepvrier, C., Pechersky, D. H., Boulin, J., Sibuet, J.-C., Savostin, L. A., Sorokhtin, L. A., Westphal, M., Bazhenov, M. L., Lauer, J. P., and Biju-Duval, B.: Geological evolution of the Tethys belt from the Atlantic to the Pamirs since the Lias, *Tectonophysics*, 123, 241–315, [https://doi.org/10.1016/0040-1951\(86\)90199-X](https://doi.org/10.1016/0040-1951(86)90199-X), 1986.
- Devoti, R., Riguzzi, F., Cuffaro, M., and Doglioni, C.: New GPS constraints on the kinematics of the Apennine subduction, *Earth Planet. Sc. Lett.*, 273, 163–174, <https://doi.org/10.1016/j.epsl.2008.06.031>, 2008.
- Doglioni, C.: A proposal for the kinematic modelling of W-dipping subductions – possible applications to the Tyrrhenian-Apennines system, *Terra Nova*, 3, 423–434, 1991.
- Doglioni, C.: Some remarks on the origin of foredeeps, *Tectonophysics*, 288, 1–20, 1993.
- Domeneghetti, A., Carisi, F., Castellarin, A., and Brath, A.: Evolution of flood risk over large areas: Quantitative assessment for the Po river, *J. Hydrol.*, 527, 809–823, 2015.
- European Commission: Urban Europe – Statistics on cities, towns and suburbs, in: *General and Regional Statistics*, edited by: Kotzeva, M., Collection: Statistical books, Luxembourg, <https://ec.europa.eu/eurostat/web/products-statistical-books/-/ks-01-16-691> (last access: 8 July 2022), 2016.
- Faccenna, C., Jolivet, L., Piromallo, C., and Morelli, A.: Subduction and the depth of convection in the Mediterranean mantle, *J. Geophys. Res.*, 108, 2099, <https://doi.org/10.1029/2001JB001690>, 2003.
- Fantoni, R. and Franciosi, R.: Mesozoic extension and Cenozoic compression in Po Plain and Adriatic foreland, *Rend. online Soc. Geol. It.*, 9, 28–31, 2009.
- Fantoni, R. and Franciosi, R.: Tectono-sedimentary setting of the Po Plain and Adriatic foreland, *Rend. Fis. Acc. Lincei*, 21, 197–209, <https://doi.org/10.1007/s12210-010-0102-4>, 2010.
- Fantoni, R. and Scotti, P.: Thermal record of the Mesozoic extensional tectonics in the Southern Alps, *Atti Ticinesi di Scienza della Terra*, 9, 96–101, 2003.
- Fantoni, R., Bersezio, R., and Forcella, F.: Alpine structure and deformation chronology at the Southern Alps-Po Plain border in Lombardy. *Bollettino della Società geologica italiana*, 123, 463–476, 2004.
- Garzanti, E., Vezzoli, G., and Andò, S.: Paleogeographic and paleodrainage changes during Pleistocene glaciations (Po Plain, northern Italy). *Earth-Sci. Rev.*, 105, 25–48, 2011.
- Ghielmi, M., Minervini, M., Nini, C., Rogledi, S., Rossi, M., and Vignolo, A.: Sedimentary and tectonic evolution in the eastern Po-Plain and northern Adriatic Sea area from Messinian to Middle Pleistocene (Italy), *Rend. Fis. Acc. Lincei*, 21, S131–S166, <https://doi.org/10.1007/s12210-010-0101-5>, 2010.
- Ghielmi, M., Minervini, M., Nini, C., Rogledi, S., and Rossi, M.: Late Miocene–Middle Pleistocene sequences in the Po Plain–Northern Adriatic Sea (Italy): the stratigraphic record of modification phases affecting a complex foreland basin, *Mar. Pet. Geol.*, 42, 50–81, <https://doi.org/10.1016/j.marpetgeo.2012.11.007>, 2013.
- Gibbard, P. L., Head, M. J., Walker, M. J. C., and Subcommission on Quaternary Stratigraphy: Formal ratification of the Quaternary System/Period and the Pleistocene Series/Epoch with a base at 2.58 Ma, *J. Quaternary Sci.*, 25, 96–102, <https://doi.org/10.1002/jqs.1338>, 2010.
- Grandić, S., Biancone, M., and Samaržija, J.: Geophysical and stratigraphic evidence of the Adriatic Triassic rift structures, *Mem. Soc. Geol. It.*, 57, 315–325, 2002.
- Helliwell, J. F. and Putnam, R. D.: Economic Growth and Social Capital in Italy, *Eastern Economic Journal*, 21, 295–307, 1995.
- Hemami, B., Masouleh, S. F., and Ghassemi, A.: 3D geomechanical modeling of the response of the Wilzetta Fault

- to saltwater disposal, *Earth Planet. Phys.*, 5, 559–580, <https://doi.org/10.26464/epp2021054>, 2021.
- Herrera-Garcia, G., Ezquerro, P., Tomás, R., Béjar-Pizarro, M., López-Vinielles, J., Rossi, M., Mateos, R. M., Carreón-Freyre, D., Lambert, J., Teatini, P., Cabral-Cano, E., Erkens, G., Galloway, D., Hung, W. C., Kakar, N., Sneed, M., Tosi, L., Wang, H., and Ye, S.: Mapping the global threat of land subsidence, *Science*, 371, 34–36, <https://doi.org/10.1126/science.abb8549>, 2021.
- International Commission on Hydrocarbon Exploration and Seismicity in the Emilia region: Report on the hydrocarbon exploration and seismicity in Emilia region, 213 pp., International Commission on Hydrocarbon Exploration and Seismicity in the Emilia region, http://mappegis.regione.emilia-romagna.it/gstatico/documenti/ICHESE/ICHESE_Report.pdf (last access: 8 July 2022), 2014.
- ISIDE Working Group: Italian Seismological Instrumental and parametric database, INGV, <http://iside.rm.ingv.it> (last access: 22 June 2021), 2010.
- ISPRA: Modello geologico 3D e geopotenziali della Pianura Padana centrale (Progetto GeoMol), Rapporti ISPRA, 234/2015, 104 pp. e Appendice, 2015.
- Kint, L., Hademenos, V., De Mol, R., Stafleu, J., Van Heteren, S., and Van Lancker, V.: Uncertainty assessment applied to marine subsurface datasets, *Q. J. Eng. Geol. Hydrogeol.*, 54, qjehg2020-028, <https://doi.org/10.1144/qjehg2020-028>, 2020.
- Lindquist, S. J.: Petroleum systems of the Po basin province of Northern Italy and the Northern Adriatic Sea: Porto Garibaldi (Biogenic), Neride/Riva di Solto (Thermal) and Marnoso Arenacea (Thermal), U. S. Department of the Interior, USGS, 1999.
- Livani, M., Scrocca, D., Arecco, P., and Doglioni, C.: Structural and stratigraphic control on salient and recess development along a thrust belt front: The Northern Apennines (Po Plain, Italy), *J. Geophys. Res.-Sol. Ea.*, 123, 4360–4387, <https://doi.org/10.1002/2017JB015235>, 2018.
- Livani, M., Scrocca, D., Gaudiosi, I., Mancini, M., Cavinato, G. P., de Franco, R., Caielli, G., Vignaroli, G., Romi, A., and Moscatelli, M.: A geology-based 3D velocity model of the Amatrice Basin (Central Italy), *Eng. Geol.*, 306, 106741, <https://doi.org/10.1016/j.enggeo.2022.106741>, 2022.
- Livani, M., Petracchini, L., Benetatos, C., Marzano, F., Billi, A., Carminati, E., Doglioni, C., Petricca, P., Maffucci, R., Codegone, G., Rocca, V., Verga, F., and Antoncicchi, I.: Digitized geological and geophysical data from the Po Plain and the northern Adriatic Sea (north Italy) collected from public sources. (Version 1.1), Zenodo [data set], <https://doi.org/10.5281/zenodo.8126519>, 2023.
- Livio, F. A., Berlusconi, A., Michetti, A. M., Sileo, G., Zerboni, A., Trombino, L., Cremaschi, M., Mueller, K., Vittori, E., Carcano, C., Rogledi, S.: Active fault-related folding in the epicentral area of the December 25, 1222 (Io = IX MCS) Brescia earthquake (Northern Italy): seismotectonic implications, *Tectonophysics*, 476, 320–335, <https://doi.org/10.1016/j.tecto.2009.03.019>, 2009.
- Maesano, F. E. and D'Ambrogio, C.: Coupling sedimentation and tectonic control: Pleistocene evolution of the central Po Basin. *Ital. J. Geosci.*, 135, 394–407, <https://doi.org/10.3301/IJG.2015.17>, 2016.
- Maesano, F. E., D'Ambrogio, C., Burrato, P., and Toscani, G.: Slip-rates of blind thrusts in slow deforming areas: Examples from the Po Plain (Italy), *Tectonophysics*, 643, 8–25, <https://doi.org/10.1016/j.tecto.2014.12.007>, 2015.
- Magistrale, H. and Day, S.: 3D simulations of multi-segment thrust fault rupture, *Geophys. Res. Lett.*, 26, 2093–2096, <https://doi.org/10.1029/1999GL900401>, 1999.
- Magistrale, H., McLaughlin, K., and Day, S.: A geology-based 3D velocity model of the Los Angeles basin sediments, *Bull. Seismol. Soc. Am.*, 86, 1161–1166, <https://doi.org/10.1785/BSSA0860041161>, 1996.
- Malinverno, A. and Ryan, W. B. F.: Extension in the Tyrrhenian Sea and shortening in the Apennines as a result of arc migration driven by sinking of the lithosphere, *Tectonics*, 5, 227–245, <https://doi.org/10.1029/TC005i002p00227>, 1986.
- Masetti, D., Fantoni, R., Romano, R., Sartorio, D., and Trevisani, E.: Tectonostratigraphic evolution of the Jurassic extensional basins of the eastern southern Alps and Adriatic foreland based on an integrated study of surface and subsurface data, *AAPG Bulletin*, 96, 2065–2089, <https://doi.org/10.1306/03091211087>, 2012.
- Molinari, I., Argnani, A., Morelli, A., and Basini, P.: Development and testing of a 3D seismic velocity model of the Po Plain sedimentary basin, Italy, *Bull. Seismol. Soc. Am.*, 105, 753–764, <https://doi.org/10.1785/0120140204>, 2015.
- Montone, P., Mariucci, M. T., Pondrelli, S., and Amato, A.: An improved stress map for Italy and surrounding regions (central Mediterranean), *J. Geophys. Res.*, 109, B10410, <https://doi.org/10.1029/2003JB002703>, 2004.
- Montone, P., Mariucci, M. T., and Pierdominici, S.: The Italian present-day stress map, *Geophys. J. Int.*, 189, 705–716, <https://doi.org/10.1111/j.1365-246X.2012.05391.x>, 2012.
- Muttoni, G., Carcano, C., Garzanti, E., Ghielmi, M., Piccin, A., Pini, R., Rogledi, S., and Sciunnach, D.: Onset of major Pleistocene glaciations in the Alps. *Geology*, 31, 989–992, <https://doi.org/10.1130/G19445.1>, (2003).
- Nicolich, R., Della Vedova, B., Giustiniani, M., and Fantoni, R.: Carta del sottosuolo della Pianura Friulana, 2004.
- Ori, G. G.: Continental depositional systems of the Quaternary of the Po Plain (northern Italy), *Sediment. Geol.*, 83, 1–14, 1993.
- Patacca, E., Sartori, R., and Scandone, P.: Tyrrhenian basin and Apenninic arcs: Kinematic relations since Late Tortonian times, *Mem. Soc. Geol. It.*, 45, 425–451, 1990.
- Pezzo, G., Petracchini, L., Devoti, R., Maffucci, R., Anderlini, L., Antoncicchi, I., Billi, A., Carminati, E., Ciccone, F., Cuffaro, M., Livani, M., Palano, M., Petricca, P., Pietrantonio, G., Riguzzi, F., Rossi, G., Sparacino, F., and Doglioni, C.: Active fold-thrust belt to foreland transition in northern Adria, Italy, tracked by seismic reflection profiles and GPS offshore data, *Tectonics*, 39, e2020TC006425, <https://doi.org/10.1029/2020TC006425>, 2020.
- Picotti, V., Capozzi, R., Bertozzi, G., Mosca, F., Sitta, A., and Tornaghi, M.: The Miocene petroleum system of the Northern Apennines in the central Po Plain (Italy), in: Thrust belts and foreland basins. From fold Kinematics to Hydrocarbon Systems, edited by: Lacombe, O., Lavé, J., Roure, F., and Vergés, J., Springer, 117–131, 2007.
- Pieri, M.: Three seismic profiles through the Po Plain, in: Seismic Expression of Structural Stiles, edited by: Bally, A. W., AAPG, Studies in Geology, 15, 8–26, 1983.

- Pieri, M. and Groppi, G.: Subsurface geological structure of the Po Plain, Italy, Progetto finalizzato Geodinamica – Sottoprogetto 5 – Modello strutturale, C.N.R., Pubbl. 414, Roma, 1981.
- Pola, M., Ricciato, A., Fantoni, R., Fabbri, P., and Zampieri, D.: Architecture of the western margin of the North Adriatic foreland: The Schio-Vicenza fault system, *Italian J. Geosci.*, 133, 223–234, 2014.
- Radwan, A. and Sen, S.: Stress Path Analysis for Characterization of In Situ Stress State and Effect of Reservoir Depletion on Present-Day Stress Magnitudes: Reservoir Geomechanical Modeling in the Gulf of Suez Rift Basin, Egypt, *Nat. Resour. Res.*, 30, 463–478, <https://doi.org/10.1007/s11053-020-09731-2>, 2021.
- Ravaglia, A., Seno, S., Toscani, G., and Fantoni, R.: Mesozoic extension controlling the Southern Alps thrust front geometry under the Po Plain, Italy: insights from sandbox models, in: *Tectonic Inversion and Structural Inheritance in Mountain Belts*, edited by: Butler, R. W. H., Tavarnelli, E., and Grasso, M., *J. Struct. Geol.*, Special Publication 28, 2084–2096, <https://doi.org/10.1016/j.jsg.2006.07.011>, 2006.
- Regione Emilia-Romagna and ENI-AGIP: Riserve Idriche Sotterranee della Regione Emilia-Romagna: A cura di G. Di Dio, S.EL.CA. s.r.l., Firenze, 120 pp., 1998.
- Regione Lombardia and ENI-AGIP: Geologia degli Acquiferi Padani della Regione Lombardia, A cura di C. Carcano & A. Piccin, S.EL.CA., Firenze, 2002.
- Ricci Lucchi, F.: The foreland basin system of the northern Apennines and related clastic wedges: A preliminary outline, *Giornale di Geologia*, 48, 165–186, 1986.
- Rio, D., Sprovieri, R., Castradori, D., and Di Stefano, E.: The Gelasian Stage (Upper Pliocene): a new unit of the global standard chronostratigraphic scale, *Episodes*, 21, 82–87, <https://doi.org/10.18814/epiugs/1998/v21i2/002>, 1998.
- Rohatgi, A.: WebPlotDigitizer user manual version 4.6, <https://automeris.io/WebPlotDigitizer/tutorial.html> (last access: 5 July 2023), 1–23, 2014.
- Rosenbaum, G. and Lister, G. S.: Neogene and Quaternary rollback evolution of the Tyrrhenian Sea, the Apennines and the Sicilian Maghrebides, *Tectonics*, 23, TC1013, <https://doi.org/10.1029/2003TC001518>, 2004.
- Rovida, A., Locati, M., Camassi, R., Lolli, B., and Gasperini, P.: The Italian earthquake catalogue CPTI15, *Bull. Earthq. Eng.*, 18, 2953–2984, <https://doi.org/10.1007/s10518-020-00818-y>, 2020.
- Rovida, A., Locati, M., Camassi, R., Lolli, B., Gasperini, P., and Antonucci, A.: Italian Parametric Earthquake Catalogue (CPTI15), versione 4.0, INGV, <https://doi.org/10.13127/CPTI/CPTI15.4>, 2022.
- Roy, M. and Clayton, R.: Crust and mantle structure beneath the Los Angeles basin and vicinity: constraints from gravity and seismic velocities, *EOS Trans. AGU*, 80, F251, 1999.
- Royden, L.: Flexural behaviour of the continental lithosphere in Italy: constraints imposed by gravity and deflection data, *J. Geophys. Res.*, 93, 7747–7766, <https://doi.org/10.1029/JB093iB07p07747>, 1988.
- Sangnimnuan, A., Li, J. W., and Wu, K.: Development of coupled two phase flow and geomechanics model to predict stress evolution in unconventional reservoirs with complex fracture geometry, *J. Petrol. Sci. Eng.*, 196, 108072, <https://doi.org/10.1016/j.petrol.2020.108072>, 2021.
- Scardia, G., De Franco, R., Muttoni, G., Rogledi, S., Caielli, G., Carcano, C., Sciunnach, D., and Piccin, A.: Stratigraphic evidence of a Middle Pleistocene climate-driven flexural uplift in the Alps, *Tectonics*, 31, TC6004, <https://doi.org/10.1029/2012TC003108>, 2012.
- Schutjens, P. M. T. M., Snippe, J. R., Mahani, H., Turner, J., Ita, J., and Mossop, A. P.: Production-induced stress change in and above a reservoir pierced by two salt domes: A geomechanical model and its implications. 72nd SPE EUROPEC/EAGE conference and exhibition, Barcelona, Spain, Extended abstracts L013, *SPE J.*, 17, 80–97, <https://doi.org/10.2118/131590-PA>, 2010.
- Scrocca, D., Carminati, E., Doglioni, C., and Marcantoni, D.: Arretramento dello slab adriatico e tettonica compressiva attiva nell'Appennino centro-settentrionale, *Rend. Soc. Geol. It.*, 2, 180–181, 2006.
- Scrocca, D., Carminati, E., Doglioni, C., and Marcantoni, D.: Slab retreat and active shortening along the central-northern Apennines, in: *Thrust Belts and Foreland Basins: From Fold Kinematics to Hydrocarbon Systems*, edited by: Lacombe, O., Lav, J., Roure, F., and Vergs, J., *Front. Earth Sci.*, Springer, 471–487, https://doi.org/10.1007/978-3-540-69426-7_25, 2007.
- Shepard, D.: A two-dimensional interpolation function for irregularly-spaced data, in: *Proceedings of the 1968 23rd ACM national conference*, 27–29 August 1968, New York, USA, 517–524, <https://doi.org/10.1145/800186.810616>, 1968.
- Süss, M. P., Shaw, J. H., Komatitsch, D., and Tromp, J.: 3D Velocity and Density Model of the Los Angeles Basin and Spectral Element Method Earthquake Simulations. American Geophysical Union, Fall Meeting 2001, abstract id. S11A-0549, 2001.
- Tabellini, G.: Culture and Institutions: Economic Development in the Regions of Europe, *J. Eur. Econ. Assoc.*, 8, 677–716, <https://doi.org/10.1111/j.1542-4774.2010.tb00537.x>, 2010.
- Tarquini, S., Isola, I., Favalli, M., and Battistini, A.: TINITALY, a digital elevation model of Italy with a 10 meters cell size (Version 1.0), INGV [data set], <https://doi.org/10.13127/TINITALY/1.0>, 2007.
- Teatini, P., Ferronato, M., and Gambolati, G.: Groundwater pumping and land subsidence in the Emilia-Romagna coastland, Italy: Modeling the past occurrence and the future trend, *Water Resour. Res.*, 42, W01406, <https://doi.org/10.1029/2005WR004242>, 2006.
- Tobler, W.: A computer movie simulating urban growth in the Detroit region, *Econ. Geogr.*, 46, 234–240, 1970.
- Toscani, G., Burrato, P., Di Bucci, D., Seno, S., and Valensise, G.: Plio-Quaternary tectonic evolution of the Northern Apennines thrust fronts (Bologna-Ferrara section, Italy): seismotectonic implications, *Ital. J. Geosci.*, 128, 605–613, 2009.
- Toscani, G., Bonini, L., Ahmad, M. I., Di Bucci, D., Di Giulio, A., Seno, S., and Galuppo, C.: Opposite verging chains sharing the same foreland: Kinematics and interactions through analogue models (Central Po Plain, Italy), *Tectonophysics*, 633, 268–282, <https://doi.org/10.1016/j.tecto.2014.07.019>, 2014.
- Turrini, C., Lacombe, O., and Roure, F.: Present-day 3D structural model of the Po Valley basin, Northern Italy, *Mar. Pet. Geol.*, 56, 266–289, <https://doi.org/10.1016/j.marpetgeo.2014.02.006>, 2014.
- Turrini, C., Angeloni, P., Lacombe, O., Ponton, M., and Roure, F.: Three-dimensional seismo-tectonics in the Po

- Valley basin, Northern Italy, *Tectonophysics*, 661, 156–79, <https://doi.org/10.1016/j.tecto.2015.08.033>, 2015.
- Turrini, C., Toscani, G., Lacombe, O., and Roure, F.: Influence of structural inheritance on foreland-foredeep system evolution: An example from the Po valley region (northern Italy), *Marine Petr. Geol.*, 77, 376–398, <https://doi.org/10.1016/j.marpetgeo.2016.06.022>, 2016.
- ViDEPI Project: Visibilità dei dati afferenti all'attività di esplorazione petrolifera in Italia, Ministero dello sviluppo economico DGRME – Società Geologica Italiana – Assomineraria, <https://www.videpi.com/videpi/videpi.asp>, (last access: 9 January 2023), 2009–2023.
- Wilson, L. F., Pazzaglia, F. J., and Anastasio, D. J.: A fluvial record of active fault-propagation folding, Salsomaggiore anticline, northern Apennines, Italy, *J. Geophys. Res.*, 114, B08403, <https://doi.org/10.1029/2008JB005984>, 2009.
- Zappaterra, E.: Carbonate paleogeographic sequences of the Periadriatic region, *Boll. Soc. Geol. It.*, 109, 5–20, 1990.
- Zerbini, S., Richter, B., Rocca, F., Van Dam, T., and Matonti, F.: A combination of space and terrestrial geodetic techniques to monitor land subsidence: case study, the Southeastern Po Plain, Italy, *J. Geophys. Res.-Sol. Ea.*, 112, B05401, <https://doi.org/10.1029/2006JB004338>, 2007.
- Zuffetti, C. and Bersezio, R.: Morphostructural evidence of late quaternary tectonics at the Po Plain-Northern Apennines border (Lombardy, Italy), *Geomorphology*, 364, 107245, <https://doi.org/10.1016/j.geomorph.2020.107245>, 2020.